Preclinical evaluation of [213]Bi-/[225]Ac-labeled low-molecular-weight compounds for radiopharmaceutical therapy of prostate cancer

Sangeeta Ray Banerjee[1,2], Ala Lisok[1], Il Minn[1], Anders Josefsson[1], Vivek Kumar[1], Mary Brummet[1], Srikanth Boinapally[1], Cory Brayton[3], Ronnie C. Mease[1,2], George Sgouros[1], Robert F. Hobbs[1,4], Martin G. Pomper[1,2]

[1]Russell H. Morgan Department of Radiology and Radiological Science; [2]Sidney Kimmel Comprehensive Cancer Center, [3]Pathology, [4]Radiation Oncology, Johns Hopkins University, School of Medicine, Baltimore, MD, USA.

Address correspondence to: Sangeeta Ray Banerjee, 1550 Orleans Street, Cancer Research Building 2, Baltimore, MD 21287, Phone:410-955-8697, email: sray9@jhmi.edu, Fax-410-614-3147

Running Title: [213]Bi-/[225]Ac-based radiotherapeutics for prostate cancer

Word Count: 6252

ABSTRACT

Prostate-specific membrane antigen (PSMA) targeted radiopharmaceutical therapy is a new treatment option for patients with advanced prostate cancer refractory to other treatments. Previously we synthesized a β-particle-emitting low-molecular-weight compound, ^{177}Lu-L1, which demonstrated reduced off-target effects in a xenograft model of prostate cancer. Here we leveraged that scaffold to synthesize α-particle-emitting analogs of L1, ^{213}Bi-L1, and ^{225}Ac-L1 to evaluate their safety and cell kill effect in PSMA+ xenograft models.

Methods: Radiochemical synthesis, cell uptake, cell kill effect, and biodistribution of ^{213}Bi-L1 and ^{225}Ac-L1 were evaluated. The efficacy of ^{225}Ac-L1 was determined in human PSMA+ subcutaneous and micrometastatic models. Subacute toxicity at 8 weeks and chronic toxicity at one year after administration were evaluated for ^{225}Ac-L1. Radiation absorbed dose of ^{225}Ac-L1 was determined using the biodistribution data and α-camera imaging.

Results: ^{213}Bi-/^{225}Ac-L1 demonstrated specific cell uptake and cell kill in PSMA+ cells. Biodistribution of ^{213}Bi-L1 and ^{225}Ac-L1 revealed specific uptake of radioactivity within PSMA+ lesions. Treatment studies of ^{225}Ac-L1 demonstrated activity-dependent, specific inhibition of tumor growth in the PSMA+ flank tumor model. ^{225}Ac-L1 also showed an increased survival benefit in the micrometastatic model compared to ^{177}Lu-L1. Activity-escalated acute and chronic toxicity studies of ^{225}Ac-L1 revealed off-target radiotoxicity, mainly in kidneys and liver. The estimated maximum tolerated activity was ~1 MBq/kg. α-camera imaging of ^{225}Ac-L1 revealed high renal cortical accumulation at 2 h followed by fast clearance at 24 h.

Conclusions: [225]Ac-L1 demonstrated activity-dependent efficacy with minimal treatment-related organ radiotoxicity issues. [225]Ac-L1 is a promising therapeutic for further clinical evaluation.

Prostate cancer (PC) is the most commonly diagnosed non-cutaneous malignancy in men, with an estimated 31,620 deaths in 2020, a 5% increase from 2019 (*1*). Prostate-specific membrane antigen (PSMA) is a well-characterized tumor marker associated with metastatic castration-resistant PC (mCRPC), the most lethal form of the disease (*2-5*). Several PSMA-targeted approaches, including small-molecule (≤ 1,000 Da) ligands, peptides, and monoclonal antibodies, have been utilized for imaging and treating patients with mCRPC (*5-7*). In particular, PSMA-based radiopharmaceutical therapy (RPT) has appeared as a promising strategy for managing patients with mCRPC (*8,9*). Coupled with PSMA-based positron emission tomography (PET) for patient selection and therapeutic monitoring, PSMA-based RPT is the treatment arm of a new radiotheranostic (*10*). To date, this approach has employed primarily agents that deliver therapeutic payloads using ^{177}Lu (half-life, 6.7 days), which emits β-particles of relatively low linear energy transfer (LET) (~0.2 keV/μm) (*11*). Along with other conventional β-particle strategies employing ^{90}Y (*12*), or ^{131}I (*13*), α-particle–emitting radionuclides are being pursued to improve efficacy, leveraging the short-range (50–100 μm), high-LET radiation (~80 keV/μm) (*14-16*).

Among the high-LET α-particle emitters, ^{225}Ac has received the most attention because of its 10-day physical half-life and high net emission energy of 27 MeV per decay (*17,18*). ^{225}Ac decays with the emission of 4 α-particles, generated by the daughter nuclides ^{221}Fr ($t_{1/2}$ = 4.8 m), ^{217}At ($t_{1/2}$ = 32 ms), ^{213}Bi ($t_{1/2}$ = 45.6 min) and ^{213}Po ($t_{1/2}$ = 4.2 μs) (*17*). Those high-LET α-particle emitting daughters have also been identified as a source of unwanted off-target radiotoxicity (*19*). For example, ^{225}Ac-PSMA-617 produced

remarkable imaging and prostate-specific antigen responses in patients with mCRPC refractory to most advanced therapies. However, it concurrently led to irreversible damage to salivary glands with attendant xerostomia (*14,20*). Additionally, although not an acute effect, over time, renal toxicity may develop as more patients are treated more frequently and are studied over longer periods (*20*). Prospective clinical data addressing that important issue are lacking for PSMA α-RPT.

Several preclinical efficacy studies employing small-molecule agents for PSMA α-RPT have appeared; however, only a few have addressed long-term and activity-limiting toxicity (*15,21-23*). Recently, we developed a series of such agents for ^{177}Lu-labeled PSMA-based RPT with the goal of reduced off-target toxicity using Glu-urea-Lys as the targeting moiety (*24*). A lead agent, ^{177}Lu-L1, demonstrated minimal chronic radiotoxicity to most normal organs, including kidneys. As a next step, here we have evaluated [225]Ac-L1 and [213]Bi-L1 (Fig.1A) in relevant tumor models. Both compounds have demonstrated specific uptake and efficacy in the PSMA+ PC3 flank tumor xenograft. We have further investigated [225]Ac-L1 for acute and chronic toxicity in immunocompetent mice and treatment efficacy in micrometastatic models. Compared to mice treated with ^{177}Lu-L1, tumor growth control was more effective in the group treated with [225]Ac-L1 in the micrometastatic model, with minimal off-target toxicity demonstrated.

MATERIALS AND METHODS

Reagents, Cell Lines and Animal Models

^{213}Bi was eluted from an ^{225}Ac-/^{213}Bi-generator following a standard operating procedure provided by the manufacturer, Oak Ridge National Laboratory. Actinium-225 nitrate was also produced by Oak Ridge National Laboratory (Oak Ridge, TN). Sublines of the androgen-independent PC3 human PC cell line, derived from advanced androgen-independent bone metastasis, were used (*25*). Six- to 8-wk-old male, nonobese diabetic/shi-scid/IL-2rgnull (NSG) mice (Johns Hopkins Animal Resources Core) were implanted subcutaneously with PSMA+ PC3 PIP (3 ×10^6) and PSMA− PC3 flu cells (1 ×10^6 in 100 µL) at the forward right and left flanks, respectively (*15,25*). Immunocompetent CD-1 mice [Crl:CD1(ICR), 8-10 weeks old, Charles River Laboratories] used for the toxicity studies. Animal studies complied with the regulations of the Johns Hopkins Animal Care and Use Committee. Compound L1 was synthesized following our recent report (*24*). Stable analogs, Bi-L1, La-L1, and Lu-L1, were prepared following the method used for radiolabeling. PSMA binding affinities of the stable analogs were determined using a fluorescence-based competitive binding assay (*25*).

Radiolabeling

Freshly eluted ^{213}Bi (18.5-30 MBq in 250 µl of a solution of 0.15 M KI in 0.1 M HCl) was added to a solution of 5-10 nmol (5-10 µl) of L1 (1 mM) and 5 µL of ascorbic acid (1.1 M) and pH was adjusted to ~4-5 using 3 M NH$_4$OAc. The solution was heated in a radiochemistry microwave chamber at 90°C for 5 min at a power of 40 watts (Resonance

Instruments Inc., Skokie, IL), and the resultant solution (~270 µL) was purified by high-performance liquid chromatography (HPLC) using a Phenomenex Luna C_{18} HPLC column (00G-4252-E0), 250×4.60 mm, 5µ, 100Å. Radiosynthesis of ^{225}Ac-L1 was also performed using microwave-assisted synthesis. In brief, to a solution of ^{225}Ac(NO$_3$)$_3$, (7.4-11.1 MBq in 10-15 µL 0.2 M HCl), was added 10 µL of ascorbic acid (1.1 M), ~10 nmol (10 µl) of L1 (1 mM), 50 µL of 0.2 M NH$_4$OAc, and 1-2 µL 5 M NH$_4$OAc to adjust to pH ~4. After microwave heating for 5 min, the solution was diluted with 200 µL of water and purified by HPLC. Flow rate was 1 mL/min with water (0.1% TFA) (A) and CH$_3$CN (0.1% TFA) (B) as the eluting solvents. To ensure highest purity, an isocratic solution of 79% A and 21% B was used to separate excess ligand from the radiolabeled compound.

Cell uptake study

Cell uptake studies were performed, as previously described (*26*). Cells (1x10^6) were incubated with 37 kBq/mL of each radiolabeled agent. To determine PSMA binding specificity, cells were pre-blocked with the known PSMA inhibitor, ZJ43 (*27*), to a final concentration of 10 µM. The obtained radioactivity values were converted into the percentage of incubated dose (%ID) per million cells.

Clonogenic survival assay

Cells (500–1,000) were seeded in 60 mm culture dishes. ^{225}Ac-L1/^{213}Bi-L1 was diluted in a prewarmed medium at different concentrations (0.04-74 kBq/mL for ^{225}Ac-L1

and 0.37-185 kBq/mL for ^{213}Bi-L1) and was incubated with the cells for 2 h. The radiolabeled compound was replaced with fresh medium, and cells were incubated for 2 wk or until colonies had ≥ 50 cells. The colonies were stained with crystal violet and counted, and the surviving fraction was normalized to the control plating efficiency (*28*). A_0 (activity to reduce survival to 37%) and 95% confidence limits of the regression fit were determined.

In vivo experiments

In vivo experiments (experiments 1-10) are summarized in Supplemental Table 1 with the relevant information.

Biodistribution

Biodistribution (Supplemental Tables 2-4) was performed following our previous report (*25*). Mice were injected via the tail vein with ^{213}Bi-L1 (185 kBq) or ^{225}Ac-L1 (18.5 kBq) (experiments 1-3). ^{225}Ac in each organ was counted 24 h after the sacrifice time to ensure complete secular equilibrium and using the ^{213}Bi energy window of 400-480 keV. Tissues were collected for histology at different time-points. Tumor sections were stained with hematoxylin and eosin (H & E), using a standard protocol. Immunohistochemical (IHC) staining was done as previously described by us (*24*) with an anti-human PSMA antibody (clone 3E6, M3620, Dako).

To determine the amount of free in vivo generated ^{213}Bi from ^{225}Ac, the kidneys and PSMA+ tumor were counted immediately after sacrifice, repeatedly using 1-minute measurement intervals at the 400-480 keV energy window for ^{213}Bi up to 5 hours after sacrifice (experiment 4). A bi-exponential expression was fitted to the decay curves obtained to determine the equilibrium ^{225}Ac and free in vivo generated ^{213}Bi at the time of sacrifice. Differences in ^{213}Bi radioactivity at the time of sacrifice and the levels from the equilibrium of ^{225}Ac reflect clearance or accumulation of ^{213}Bi. The time-activity curves of free ^{213}Bi were then constructed with free ^{213}Bi activities at multiple sacrifice time-points.

Dosimetry and α-camera imaging

Normal tissue and tumor absorbed dose coefficients (ADCs) were estimated for ^{225}Ac-L1 after accounting for the α-radiation deposited locally within the mouse according to an established method (29). Only α-particle emission was considered in the calculations. It was assumed to be deposited locally with the absorbed fraction, φ=1, for both the parent ^{225}Ac and all of the radioactive daughters, except for the kidneys, as mentioned earlier, where absorbed dose from additional free ^{213}Bi was tabulated. Potential human ADCs were estimated by using a standard mouse-to-human conversion formula for time-integrated activities (30) that were then input to OLINDA/EXM 1.0 version (31).

Digital autoradiography was performed using the α-camera (32) to visualize the activity and distribution activities at sub-tissue levels. After administration of ^{225}Ac-L1 (0.4

MBq) via tail-vein injection, the mice were sacrificed at 2 and 24 h (n=2) (experiment 5). Kidneys, salivary glands, and tumors were harvested and immediately embedded in optimal cutting temperature compound, frozen on dry ice and cryostat-sectioned in 8 μm sections. Image analysis was performed using ImageJ Fiji (version 1.49g, NIH). The relative ^{225}Ac-L1 activity concentrations in the sub-tissue level versus the average of the whole tissue sample were calculated.

Radiopharmaceutical therapy

Efficacy in a flank xenograft model. Mice were injected subcutaneously within the flank with $2×10^6$ PSMA+ PC3 PIP or $1× 10^6$ PSMA− PC3 flu cells. Treatments (^{213}Bi-L1, and ^{225}Ac-L1, experiments 6-7) were conducted 12-15 d later when tumor volume was less than 100-150 mm^3. Tumors were then measured 2–3 times per wk until they reached 1,000 mm^3. Three mice from each group (n=3 per group) were removed to evaluate acute toxicity after 8 wk.

Efficacy in a micrometastatic model. PC3-ML-fLuc-PSMA cells were maintained as described previously (*21*). Briefly, mice were injected intravenously with $1×10^6$ PC3-ML-fLuc-PSMA cells (experiment 8A). One day later, mice were injected intravenously with 93 kBq of ^{225}Ac-L1 (group 1) and with the fractionated activity of 9.3 kBq at 48 h interval [group 2 (×4), group 3 (×6) and group 4 (×8), and control group (0 kBq)]. Metastatic tumor progression was monitored by in vivo bioluminescence imaging (IVIS Spectrum; Perkin-Elmer, Waltham, MA) and survival. A second study was performed in

a micrometastatic model (experiment 8B) using ^{225}Ac-L1, 37 kBq, and 74 kBq and ^{177}Lu-L1 (37 MBq) and control group (0 kBq).

Toxicity and maximum tolerated activity. The maximum tolerated activity (MTA) was defined as the highest activity at which no animal died or lost more than 20% of its pre-treatment weight. Mice (bodyweight 34.9±0.5 gm) were weighed and inspected twice per wk for at least 12 mo. A toxicity study was also performed using the fractionated activity scheme applied for the micrometastatic model [0, 93 kBq, 9.3 kBq×4, 9.3 kBq×6, and 9.3 kBq×8] (experiment 9). A separate study (experiment 10) was also performed, administered intravenously of 18.5 kBq×2 (group 1) and 37 kBq×2 (group 2) of ^{225}Ac-L1, selected based on the activity used for the treatment of flank tumor model. The control group (group 3) received only saline vehicle. On sacrifice, animals were evaluated by the Johns Hopkins Phenotyping Core. Complete blood count (CBC), serum chemistry, necropsy, and histopathology (>30 tissues) were performed. Urinalysis (Chemstrip® Test Strips - Roche Diagnostics) for specific gravity and protein was performed monthly for each animal.

Statistical analysis

Statistical significance was calculated using an unpaired two-tailed t-test. Analysis of Kaplan–Meier curves and survival comparisons were performed using the Log-Rank test.

RESULTS

Radiolabeling

We developed a fast microwave-assisted radiolabeling method to synthesize ^{213}Bi-L1 and ^{225}Ac-L1 with high yield (>70%) and purity (>98%) and with molar activity >8.9 MBq/nmol. The HPLC method also enabled the separation of ^{213}Bi-L1 from ^{225}Ac-L1 and the excess ligand due to their different retention times. ^{213}Bi-L1 is assumed to be generated from starting ^{225}Ac(NO$_3$)$_3$ that had ^{213}Bi as the decay product. Because actinium has no stable isotope, we have evaluated several conventional surrogates, Bi-L1, La-L1, and Lu-L1, as reference compounds for HPLC (Supplemental Figs. 1-3). ^{225}Ac-L1 demonstrated a longer retention time than those surrogate compounds. PSMA binding affinities (K_i) of stable analogs ranged from 0.1-5.1 nM. *In cellulo* experiments demonstrated high and specific cell uptake and killing efficiency for both ^{213}Bi-L1 and ^{225}Ac-L1 in PSMA+ PC3 PIP cells (Fig. 1B). PSMA− PC3 flu cells were insensitive to either compound under similar conditions. ^{225}Ac-L1 (D_0 9-12 kBq/mL) was more effective than ^{213}Bi-L1 (95-122 kBq/mL) in PSMA+ cells (Fig. 1B).

Biodistribution

Biodistribution of ^{213}Bi-L1 (Fig. 2A, experiment 1) was determined up to 2 h, considering its short half-life. High PSMA+ PC3 PIP tumor uptake was observed as early as 10 min post-injection, 18.9±3.1 %ID/g, and increased to 29.4±8.0 %ID/g at 2 h. The agent displayed rapid clearance from blood, showing 5.1±1.7 %ID/g at 10 min dropping to 0.57±0.0 %ID/g at 2 h. Renal uptake was 49.0±21.2 %ID/g at 10 min and displayed rapid clearance to 23.1±6.7, 9.9±1.8, and 8.6±3.0 %ID/g at 30 min, 1 h, and 2 h,

respectively. Activity accumulation in the heart, liver, spleen, and salivary glands were found <1% ID/g after 2 h.

Biodistribution of ^{225}Ac-L1 was performed up to 8 d after administration (Fig. 2A, experiment 2). ^{225}Ac-L1 was cleared rapidly from the blood pool, (<0.5 %ID/g all time-points) and efficiently accumulated in the PSMA+ tumor to 45.8±17.9 %ID/g at 2 h, 44.5 ±12.9 %ID/g at 8 h, and remained high at 49.0±17.9 %ID/g at 24 h. Clearance from tumor was protracted at 22.0±7.5 %ID/g at 48 h, 18.3±4.1 %ID/g at 72 h, 19.2±6.4 %ID/g at 96 h, 12.6±3.2 %ID/g at 120 h and 10.0±2.2 %ID/g at 8 d post-injection. Renal uptake was highest at 2 h, at 27.5±14.9 %ID/g, followed by relatively rapid clearance to 3.1±0.9 % ID/g at 8 h and 1.5±0.5 %ID/g at 24 h, dropping below 1% at later times. Tumor-to-kidney ratios increased from 79.3±25.0 at 2 h to 314.5±185.8 at 8 h, 203.8±123.1 at 24 h, 101.0±64.3 at 48 h, 242.5±107.8 at 72 h, 168.7±33.5 at 96 h, 147.9±40.2 at 120 h, and 148±75 at 8 d. Biodistribution beyond 8 d was not performed due to a significant reduction in PSMA+ tumor volume.

Among normal organs liver displayed moderate uptake at 8 h (3.9±1.1 %ID/g) and remained at that level at 24 h (3.1±0.8 %ID/g), decreasing to 2.1±0.4 %ID/g at 8 days post-injection. Accordingly, a biodistribution study was performed in tumor-free CD-1 mice to determine whether liver retention was related to the animal model or if there were any chemical instability of ^{225}Ac-L1 in vivo (experiment 4). Our previous studies revealed significantly higher liver uptake in immunodeficient, tumor-bearing NSG mice compared to immunocompetent CD-1 mice when administered with the anti-PSMA antibody, ^{111}In-

5D3 (*33*). Consistent with the previous report, [225]Ac-L1 also displayed significantly lower liver uptake (≤1% ID/g) at all time-points in CD-1 mice. Blood uptake and all other normal tissues showed low uptake (<1%) after 8 h.

Morphological changes of the tissues were evaluated by H&E staining (Fig. 2B). Whole tumor H&E staining at 96 h and 8 d displayed necrosis within the treated tumors. PSMA IHC within the PSMA+ PC3 PIP tumors revealed a decrease in PSMA expression at 24-192 h compared to tumor harvested from control animals that did not receive radioactivity. That could be attributed to a treatment effect that resulted in a decrease in PSMA+ tumor cells with time.

Radiopharmaceutical therapy

Anti-tumor effect in the flank tumor model. Study design and activity-dependent treatment effects of [225]Ac-L1 in this model are shown in Fig. 3 (experiment 7). The control groups [untreated PSMA+ or PSMA− and the PSMA− tumor-bearing group with 18.5 kBq×2] did not show any significant difference in time to reach a 10-fold increase from the initial tumor volume ($V_t/V_0 \leq 10$) with median survival 17 d. Animals receiving any single dose or two fractionated doses (7 d apart) demonstrated significant tumor growth delay in PSMA+ tumors ($P < 0.003$) compared to the control groups. However, slow tumor regrowth was observed after 8 wk for the treatment groups that received 9.3 kBq×1 and 9.3 kBq×2 doses. In contrast, a durable treatment effect was recorded when PSMA+ PIP-bearing animals received 18.5 kBq×2 (Fig. 3B), where median $V_t/V_0 \leq 10$ was 168d.

Significantly, while the single administration of 18.5 kBq resulted in an increase of $V_t/V_0 > 10$ within 8 wk for three mice from this group, the remaining two mice displayed significant tumor growth control and increased bodyweight recovery indicating relatively lower radiotoxicity compared to the rest of the treated groups. The median time to reach a $V_t/V_0 \leq 10$ is listed in Fig. 3B. A preliminary efficacy study was also performed with [213]Bi-L1 (3.7MBq). It showed expected tumor control [$V_t/V_0 \leq 10$ (35d)] compared to the untreated group (15 d) (Supplemental Fig. 4) in the PSMA+ flank tumor model.

Anti-tumor effect in the PSMA(+) micrometastatic model. The study design and efficacy of [225]Ac-L1 as single and fractionated activity were shown in Fig. 4A. (experiment 8A). Mice that received 9.3 kBq×6 of [225]Ac-L1 demonstrated the highest survival (P <0.002), with a median survival of 72 d compared to the untreated group, 44 d, from initiation of the experiment.

A separate experiment was performed to compare the effect of a single administration of [225]Ac-L1 with that of ^{177}Lu-L1 (37 MBq) (Fig. 4B, experiment 8B). No survival benefit for the group treated with ^{177}Lu-L1 was observed compared to the untreated group, with median survival times of 46 and 47 days, respectively. In contrast, [225]Ac-L1 (37 kBq and 74 kBq) displayed significantly increased survival over controls (P < 0.001).

In vivo radiotoxicity and MTA. Study design of the chronic and acute toxicity studies are shown in Figs. 5A-B (experiments 9-10). Acute toxicity of [225]Ac-L1 was

evaluated in tumor-bearing NSG mice after 8 wk and tumor-free CD-1 mice. In general, blood counts and chemistry (Supplemental Tables 6-7) were not significantly affected acutely compared to untreated, control mice.

A chronic toxicity study was performed following the fractionated dosage scheme (Fig. 5A) used for the micrometastatic model, which assessed the long-term effects of ^{225}Ac-L1 (Figs. 5B, Supplemental Table 8). All mice treated with 93 kBq (n = 5/5) and 9.3 kBq×4 survived for over 12 months. Significantly, all treated mice displayed acceptable hematologic changes compared to the untreated mice. Moderate changes in creatinine and blood urea alanine levels (for kidney function) were seen only for the higher treatment groups with renal cortical changes (H&E) not seen in the control group (Supplemental Fig. 6). Elevated values of aspartate aminotransferase (AST), alanine aminotransferase (ALT), and gamma-glutamyl transferase (GGT) were consistent with liver toxicity in these two groups.

Limited chronic toxicity was also performed following the activity used for flank tumor models (experiment 10). While 3 out of 5 CD-1 mice treated with 18.5 kBq×2 survived after 12 mo (Supplemental Table 9), the group treated with 37 kBq×2 showed significant weight loss after 6 mo. All mice from that latter group were removed from the study to evaluate the activity-limiting toxicity. Elevated AST, ALT, and GGT were consistent with liver damage in treated animals, as seen from experiment 9. Parotid glands in treated animals displayed small acini and higher cytoplasmic variation compared to controls after one-year for mice treated with 18.5 kBq×2 (Supplemental Fig.

7). There are more cytoplasmic variation and anisocytosis in the lacrimal glands tissue in 2 treated mice.

In summary, based on the chronic toxicity studies, MTA was conservatively determined as the fractionated administration of 9.3 kBq×4. The fractionated dosage of 18.5 kBq×2 may also be considered safe. Two mice that died at month 10-11 were not available for pathologic assessment. Lung tumors <5 mm diameter were identified in 2 treated animals from the chronic toxicity studies. Such spontaneous tumorigenesis (adenoma of lung and liver) is the common cause of death for older CD-1 mice (*34-36*).

Alpha camera imaging and dosimetry

Figs. 6A-B provide a selected list of the murine ADCs. PSMA+ PC3 PIP tumors received the highest ADC (680 mGy/kBq), followed by liver (94 mGy/kBq) and kidney (82 mGy/kBq). Absorbed doses of other normal tissues were low. Therapeutic ratios of PSMA+ tumor-to-normal organs were calculated for selected organs (Fig. 6B). Therapeutic ratios were high and followed the order: bone marrow (1115)>>salivary gland (123)> blood(40)> kidney(8.3) and liver(7.2), indicating either kidney or liver as the absorbed dose-limiting organ. Estimated human average organ ADCs from OLINDA/EXM, based on mouse-to-human time-integrated activity conversion for selected organs, are listed in Supplemental Table 5.

Distribution of radioactivity within the tumor, kidney, and salivary glands was further evaluated ex vivo by α-camera imaging at 2 and 24 h after treatment (Fig. 6C,

experiment 5). The kidney displayed a highly heterogeneous intra-organ distribution of radioactivity, with preferential renal cortical accumulation as anticipated due to high levels of PSMA within this region (*37*) as well as the accumulation of free ^{213}Bi (*38*). Rapid clearance of ^{225}Ac was observed after 24 h, consistent with the biodistribution data, and further reflecting favorable pharmacokinetics of ^{225}Ac-L1. The ratio of signal intensity within the renal cortex to that of the medulla was 4:1 at 2 h. A uniform distribution of radioactivity was noted in PSMA+ tumor at both time-points, indicating sufficient internalization of ^{225}Ac after 24 h to produce an anti-tumor effect. Non-uniform distribution of radioactivity within the salivary glands was found for both parotid and submandibular glands at 2 h, with radioactivity levels too low to enable imaging at 24 h.

DISCUSSION

PSMA α-RPT holds great potential as a safe and effective treatment option in patients with mCRPC. Although α-RPT with [225]Ac-PSMA-617 has demonstrated substantial responses, salivary gland radiotoxicity has curtailed further adoption of this agent (*20*). Here we report a detailed preclinical investigation of a new [225]Ac-labeled compound, with attention to radiolabeling method, biodistribution, efficacy in two human tumor models, radiotoxicity, and α-camera-guided dosimetry. The goal was to provide an [225]Ac-labeled compound that might be as or more effective than existing agents, but with fewer off-target effects.

Since the initial demonstration of [213]Bi-labeled and, more recently, [227]Th-labeled anti-PSMA-antibodies for α-RPT (*39,40*), several low-molecular-weight PSMA α-RPT have been developed preclinically for their fast and favorable pharmacokinetics as demonstrated clinically by [225]Ac-PSMA-617 (*14*). Unconventional radioisotopes to enable concurrent PET imaging (*41*) or efforts to improve the therapeutic window, often at the expense of increased retention in the blood (*23*), have been pursued. Studies are also directed towards developing a more relevant tumor model to address PSMA heterogeneity, which has been demonstrated in the clinical setting (*42*). It is challenging to compare the safety and efficacy of those reported compounds with [225]Ac-L1 because of the different tumor models and murine species involved, and the lack of readily available long-term toxicity data in the literature. We did not perform detailed safety and efficacy studies for [213]Bi-L1 due to the inconveniently short half-life of [213]Bi, and the sense that if we were to move forward clinically, it would be with [225]Ac-L1 or a close analog.

There are several key outcomes from this work: First, we presented an optimized radiosynthesis method to provide the highest possible molar specificity for ^{225}Ac-L1. Second, we used biodistribution studies together with α-camera-guided dosimetry to uncover the dose-limiting organ, which could be kidney or liver, and less likely, bone marrow. The data were supported by long-term radiotoxicity studies, which revealed that the liver and less likely kidney was the dose-limiting organ. Notably, while a high single-dose of ^{177}Lu-L1 (111 MBq) did not generate renal or hematologic toxicity after one-year of follow-up (*24*), ^{225}Ac-L1 indeed displayed typical renal cortical damage at the higher doses, 4×9.3 kBq was considered the MTA. Third, consistent with our previous report on ^{212}Pb-based α-RPT (*15*), the data also revealed a superior efficacy of α-RPT compared to β-RPT (^{177}Lu-L1) in treating micrometastatic disease. Considering the energy ratio of ^{225}Ac (27 MBq)-to-^{177}Lu (0.4 MBq) of 70-to-1, ^{225}Ac-L1 (4×9.3 kBq) demonstrated an ~10-12 d survival benefit using a safe dose at the MTA compared to ^{177}Lu-L1 (37 MBq). The administered dose of ^{177}Lu-L1 was 14-fold higher compared to ^{225}Ac-L1. Notably, a short half-life ^{211}At-labeled compound displayed significantly higher survival benefit compared to ^{225}Ac-L1, although long-term toxicity data revealed severe renal cortical damage after 10 months post-treatment (*21*). That finding underlines the potential advantage of ^{225}Ac α-RPT, even with concerns related to its α-emitting daughters. Fifth, low tumor-to-liver ratios were found for ^{225}Ac-L1, which we believe are most likely associated with the use of immunocompromised NSG mice combined with the release of decayed daughters within the liver. Mild hepatobiliary radiotoxicity was also identified in long-term toxicity with higher doses of ^{225}Ac-L1 but not with ^{177}Lu-L1.

Human MTAs based on whole organ dosimetry are 140 MBq for the liver as the dose-limiting organ and 130 MBq for the kidney, assuming a global relative biological effect (RBE) of 5 relative to external beam thresholds in units of 2-Gy fraction equivalent of external beam radiation (Supplemental Table 5C). However, liver dosimetry included all daughters from the ^{225}Ac decay chain, which is undoubtedly an overestimation of the absorbed dose as the liver is the likely source of the free daughters (^{221}Fr and ^{213}Bi) seen to accumulate in the kidney. Conversely, the kidney absorbed dose value is likely an underestimation in terms of toxicity threshold assessment as the activity was localized to portions of the cortex, most likely the proximal tubules, such that a possible factor of ~4 of dose concentration for the average organ dose may be present based on α-camera imaging data. A full dosimetric analysis of these and the value of sub-organ RBE representing the radiobiological effects of α-particles is beyond the scope of this article. Regardless, projections of activity limits to humans from the murine studies are highly uncertain, and any clinical application should be carried out in dose increments from values well below the calculated MTA.

We recognize that the high levels of PSMA in the PSMA+ PC3 PIP tumor xenograft presents an unnatural situation, a limitation of our studies. A recent report by Current et al. using variable ratios of PSMA+ PC3 PIP with PSMA− PC3 flu cells might address the issue (*42*). Based on Current et al.'s data, the efficacy of PSMA α-RPT is positively correlated to the PSMA expression/cell and the fraction of PSMA+ cells per lesion. The

number of PSMA receptors per PC3 PIP cell was measured at ~5.5 ×10^5 (flow cytometry). Based on our study, ^{225}Ac-L1 could provide a curative dose of 50 Gy for the PSMA+ PC3 PIP tumor with an estimated dose of 31 MBq (Supplemental Table 5C). Additionally, our preclinical long-term toxicity study (extrapolated from 35 gm mouse to 73.7 kg adult human male) revealed that the MTA for an adult human male is estimated to be ~77 MBq. Accordingly, ~ 2.2 x 10^5 PSMA receptors per cell would be treated safely using ^{225}Ac-L1 as a standalone therapy and is in the range of PSMA expression on the human PC cell lines, C4-2 (*42*) and LNCaP (*43*).

Another limitation of our study is using a small number of control animals for toxicity studies. That situation was associated with the unexpected death of the treated mice during the one-year-long toxicity studies, with matched control mice sacrificed to enable comparison of radiotoxicity. Such long-term radiotoxicity studies with more control animals will be important to initiate clinical translation of the studied α-RPT agents.

CONCLUSION

We have evaluated new PSMA-based α-RPT agents ^{213}Bi-L1 and ^{225}Ac-L1. ^{225}Ac-L1 demonstrated PSMA-specific tumor growth delay in both large and micrometastatic tumor models without causing off-target toxicity using fractionated activity administration. Results suggest testing ^{225}Ac-L1 in patients with mCRPC.

DISCLOSURE

ACKNOWLEDGEMENTS

KEY POINTS:

QUESTION: Can we deliver PSMA-targeted α-RPT using ^{225}Ac-labeled, low-molecular-weight radioligands to tumor-bearing mice safely and with high efficacy?

PERTINENT FINDINGS: We investigated an optimized ^{225}Ac-labeled PSMA-targeted compound,^{225}Ac-L1, which safely demonstrated tumor growth control in both flank and micrometastatic models, and did so more effectively than the corresponding ^{177}Lu-labeled analog. Our data indicate that it is possible to provide a safe and therapeutically effective dose of ^{225}Ac-L1.

IMPLICATIONS FOR PATIENT CARE: ^{225}Ac-L1, designed to mitigate off-target effects, is a promising candidate for clinical PSMA-targeted α-RPT.

REFERENCES

1.   Key statistics for prostate cancer. American Cancer Society. <https://www.cancer.org/cancer/prostate-cancer/about/key-statistics.html>. Accessed 10/9/2020.

2.   Silver DA, Pellicer I, Fair WR, Heston WD, Cordon-Cardo C. Prostate-specific membrane antigen expression in normal and malignant human tissues. *Clin Cancer Res.* 1997;3:81-85.

3.   Sweat SD, Pacelli A, Murphy GP, Bostwick DG. Prostate-specific membrane antigen expression is greatest in prostate adenocarcinoma and lymph node metastases. *Urology.* 1998;52:637-640.

4.   Haberkorn U, Eder M, Kopka K, Babich JW, Eisenhut M. New strategies in prostate cancer: Prostate-specific membrane antigen (PSMA) ligands for diagnosis and therapy. *Clin Cancer Res.* 2016;22:9-15.

5.   Kiess AP, Banerjee SR, Mease RC, et al. Prostate-specific membrane antigen as a target for cancer imaging and therapy. *Q J Nucl Med Mol Imaging.* 2015;59:241-268.

6.   Morris M, Vogelzang NJ, Sartor O, et al. 793PD - Phase 1 study of the PSMA-targeted small-molecule drug conjugate EC1169 in patients with metastatic castrate-resistant prostate cancer (mCRPC). *Ann Oncol.* 2017;28:v273.

7.   Rahbar K, Ahmadzadehfar H, Kratochwil C, et al. German multicenter study investigating ^{177}Lu-PSMA-617 radioligand therapy in advanced prostate cancer patients. *J Nucl Med.* 2017;58:85-90.

8.   Hofman MS, Violet J, Hicks RJ, et al. ^{177}Lu-PSMA-617 radionuclide treatment in patients with metastatic castration-resistant prostate cancer (LuPSMA trial): a single-centre, single-arm, phase 2 study. *Lancet Oncol.* 2018;19:825-833.

9.   Hofman MS, Lawrentschuk N, Francis RJ, et al. Prostate-specific membrane antigen PET-CT in patients with high-risk prostate cancer before curative-intent surgery or radiotherapy (proPSMA): a prospective, randomised, multicentre study. *Lancet.* 2020;395:1208-1216.

10.   Herrmann K, Schwaiger M, Lewis JS, et al. Radiotheranostics: A roadmap for future development.

11.   Kassis AI. Therapeutic radionuclides: biophysical and radiobiologic principles. *Semin Nucl Med.* 2008;38:358-366.

12.   Rathke H, Flechsig P, Mier W, et al. Dosimetry estimate and initial clinical experience with ^{90}Y-PSMA-617. *J Nucl Med.* 2019;60:806-811.

13.   Zechmann CM, Afshar-Oromieh A, Armor T, et al. Radiation dosimetry and first therapy results with a ^{124}I/^{131}I-labeled small molecule (MIP-1095) targeting PSMA for prostate cancer therapy. *Eur J Nucl Med Mol Imaging.* 2014;41:1280-1292.

14.   Kratochwil C, Bruchertseifer F, Rathke H, et al. Targeted alpha therapy of mCRPC with ^{225}Actinium-PSMA-617: Dosimetry estimate and empirical dose finding. *J Nucl Med.* 2017.

15.   Banerjee SR, Minn I, Kumar V, et al. Preclinical evaluation of $^{203/212}$Pb-labeled low-molecular-weight compounds for targeted radiopharmaceutical therapy of prostate cancer. *J Nucl Med.* 2020;61:80-88.

16.   Sathekge M, Bruchertseifer F, Vorster M, et al. Predictors of overall and disease-free survival in metastatic castration-resistant prostate cancer patients receiving ^{225}Ac-PSMA-617 radioligand therapy. *J Nucl Med.* 2020;61:62-69.

17.   Scheinberg DA, McDevitt MR. Actinium-225 in targeted alpha-particle therapeutic applications. *Curr Radiopharm.* 2011;4:306-320.

18.   Morgenstern A, Apostolidis C, Kratochwil C, Sathekge M, Krolicki L, Bruchertseifer F. An overview of targeted alpha therapy with ^{225}Actinium and ^{213}Bismuth. *Curr Radiopharm.* 2018;11:200-208.

19.   Song H, Hobbs RF, Vajravelu R, et al. Radioimmunotherapy of breast cancer metastases with alpha-particle emitter ^{225}Ac: comparing efficacy with ^{213}Bi and ^{90}Y. *Cancer Res.* 2009;69:8941-8948.

20.   Langbein T, Chaussé G, Baum RP. Salivary gland toxicity of PSMA radioligand therapy: relevance and preventive strategies. *J Nucl Med.* 2018;59:1172-1173.

21. Kiess AP, Minn I, Vaidyanathan G, et al. (2S)-2-(3-(1-Carboxy-5-(4-[211]At-astatobenzamido)pentyl)ureido)-pentanedioic acid for PSMA-targeted α-particle radiopharmaceutical therapy. *J Nucl Med.* 2016;57:1569-1575.

22. Nonnekens J, Chatalic KL, Molkenboer-Kuenen JD, et al. [213]Bi-labeled prostate-specific membrane antigen-targeting agents induce DNA double-strand breaks in prostate cancer xenografts. *Cancer Biother Radiopharm.* 2017;32:67-73.

23. Kelly JM, Amor-Coarasa A, Ponnala S, et al. A single dose of [225]Ac-RPS-074 induces a complete tumor response in an lncap xenograft model. *J Nucl Med.* 2019;60:649-655.

24. Banerjee SR, Kumar V, Lisok A, et al. ^{177}Lu-labeled low-molecular-weight agents for PSMA-targeted radiopharmaceutical therapy. *Eur J Nucl Med Mol Imaging.* 2019;46:2545-2557.

25. Banerjee SR, Pullambhatla M, Byun Y, et al. Sequential SPECT and optical imaging of experimental models of prostate cancer with a dual modality inhibitor of the prostate-specific membrane antigen. *Angew Chem Int Ed.* 2011;50:9167-9170.

26. Ray Banerjee S, Chen Z, Pullambhatla M, et al. Preclinical comparative study of ^{68}Ga-labeled DOTA, NOTA, and HBED-CC chelated radiotracers for targeting PSMA. *Bioconjugate Chemistry.* 2016;27:1447-1455.

27. Olszewski RT, Bukhari N, Zhou J, et al. NAAG peptidase inhibition reduces locomotor activity and some stereotypes in the PCP model of schizophrenia via group II mGluR. *J Neurochem.* 2004;89:876-885.

28. Franken NAP, Rodermond HM, Stap J, Haveman J, van Bree C. Clonogenic assay of cells in vitro. *Nat Protoc.* 2006;1:2315-2319.

29. Bolch WE, Eckerman KF, Sgouros G, Thomas SR. MIRD Pamphlet No. 21: A generalized schema for radiopharmaceutical dosimetry—standardization of nomenclature. *J Nucl Med.* 2009;50:477-484.

30. Josefsson A, Nedrow JR, Park S, et al. Imaging, biodistribution, and dosimetry of radionuclide-labeled PD-L1 antibody in an immunocompetent mouse model of breast cancer. *Cancer Res.* 2016;76:472-479.

31. Stabin MG, Sparks RB, Crowe E. OLINDA/EXM: The second-generation personal computer software for internal dose assessment in nuclear medicine. *J Nucl Med.* 2005;46:1023-1027.

32. Bäck T, Jacobsson L. The α-camera: A quantitative digital autoradiography technique using a charge-coupled device for ex vivo high-resolution bioimaging of α-particles. *J Nucl Med.* 2010;51:1616-1623.

33. Ray Banerejee S, Kumar V, Lisok A, et al. Evaluation of ^{111}In-DOTA-5D3, a surrogate SPECT imaging agent for radioimmunotherapy of prostate-specific membrane antigen. *J Nucl Med.* 2018.

34. Brayton CF, Treuting PM, Ward JM. Pathobiology of aging mice and GEM: background strains and experimental design. *Vet Pathol.* 2012;49:85-105.

35. Engelhardt JA, Gries CL, Long GG. Incidence of spontaneous neoplastic and nonneoplastic lesions in Charles River CD-1 mice varies with breeding origin. *Toxicol Pathol.* 1993;21:538-541.

36. Engelhardt JA, Gries CL, Long GG. Incidence of Spontaneous Neoplastic and Nonneoplastic Lesions in Charles River CD-1® Mice Varies with Breeding Origin. *Toxicologic Pathology.* 1993;21:538-541.

37. Bacich DJ, Pinto JT, Tong WP, Heston WDW. Cloning, expression, genomic localization, and enzymatic activities of the mouse homolog of prostate-specific membrane antigen/NAALADase/folate hydrolase. *Mamm Genome.* 2001;12:117-123.

38. Miederer M, McDevitt MR, Sgouros G, Kramer K, Cheung N-KV, Scheinberg DA. Pharmacokinetics, dosimetry, and toxicity of the targetable atomic generator, [225]Ac-HuM195, in nonhuman primates. *J Nucl Med.* 2004;45:129-137.

39. McDevitt MR, Barendswaard E, Ma D, et al. An α-particle emitting antibody ([213]Bi-J591) for radioimmunotherapy of prostate cancer. *Cancer Res.* 2000;60:6095-6100.

40. Hammer S, Hagemann UB, Zitzmann-Kolbe S, et al. Preclinical efficacy of a PSMA-targeted thorium-227 conjugate (PSMA-TTC), a targeted alpha therapy for prostate cancer. *Clin Cancer Res.* 2020;26:1985-1996.

41.   Umbricht CA, Köster U, Bernhardt P, et al. Alpha-PET for prostate cancer: preclinical investigation using ^{149}Tb-PSMA-617. *Sci Rep.* 2019;9:17800.

42.   Current K, Meyer C, Magyar CE, et al. Investigating PSMA-targeted radioligand therapy efficacy as a function of cellular PSMA levels and intra-tumoral PSMA heterogeneity. *Clin Cancer Res.* 2020:In Press. .

43.   Lückerath K, Stuparu AD, Wei L, et al. Detection Threshold and Reproducibility of (68)Ga-PSMA11 PET/CT in a Mouse Model of Prostate Cancer. *J Nucl Med.* 2018;59:1392-1397.
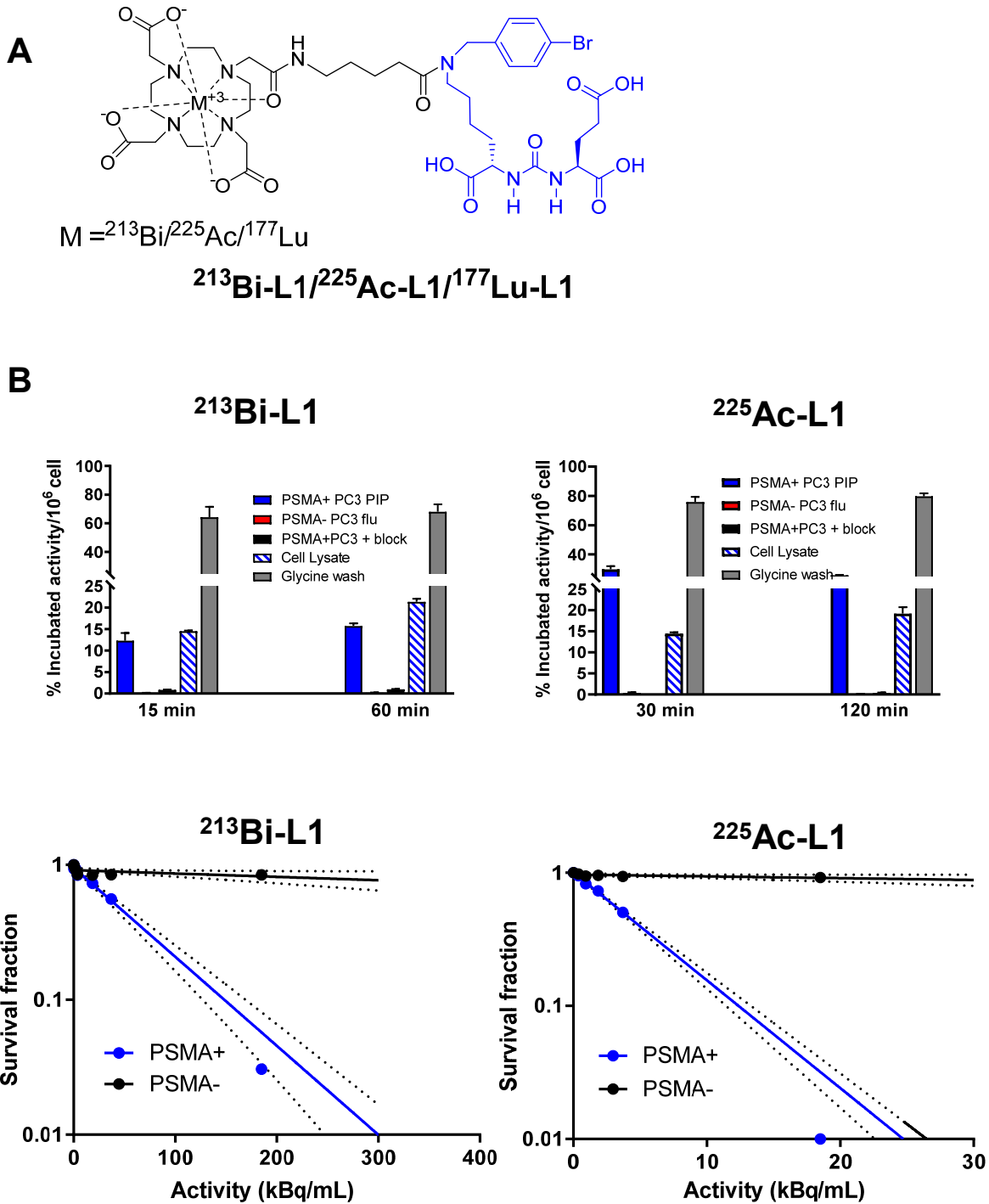
Figure 1. A. Chemical structures of [213]Bi-L1 and [225]Ac-L1; **B.** Cell uptake and internalization (top) (mean±SD, n=3) and cell kill effect (bottom) in PSMA+ PC3 PIP and PSMA- PC3 flu cells after 2 h of incubation; at 37°C. Dashed line indicates 95% confidence limit for regression fit
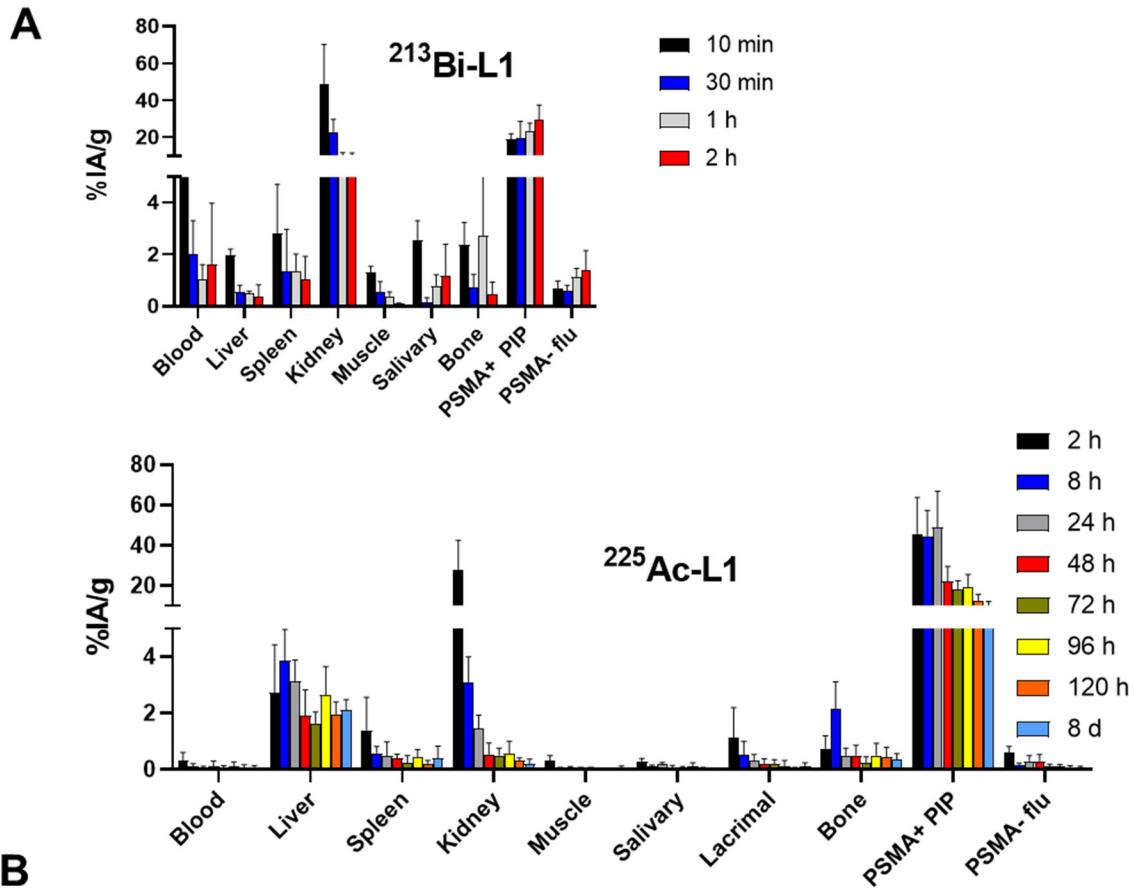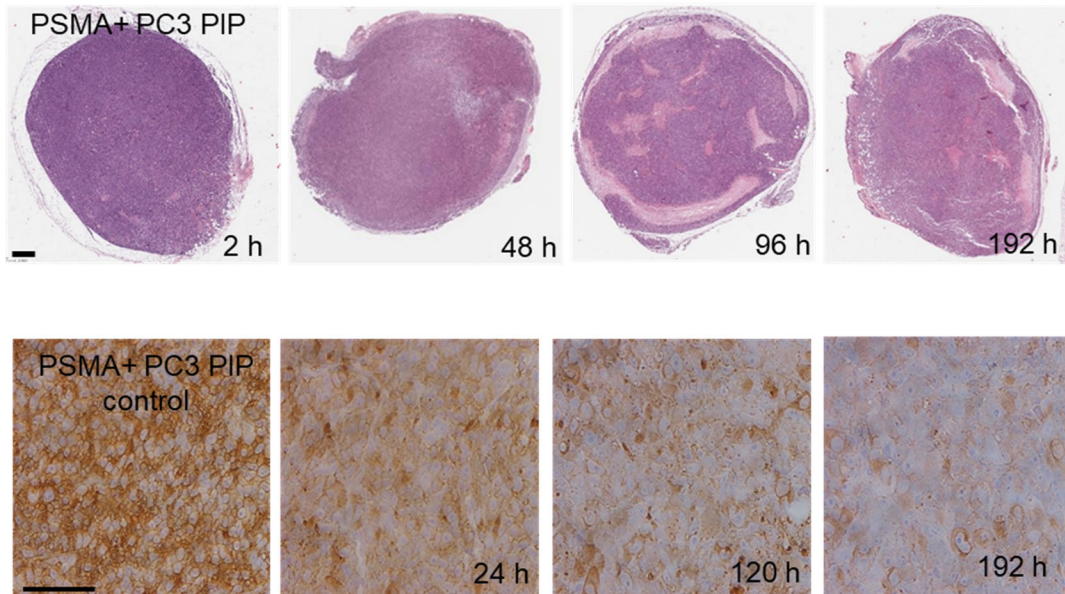
Figure 2. A. Biodistribution data of ^{213}Bi-L1 and ^{225}Ac-L1, %Injected activity (IA)/g, mean±SD, n=4); **B.** Ex vivo staining: PSMA+ PC3 PIP tumor after administration of ^{225}Ac-L1 H&E (top), scale bar:1.2 mm, 2×; PSMA+ PIP tumor, PSMA immunohistochemistry (scale bar:50 µm, 20×) (bottom).
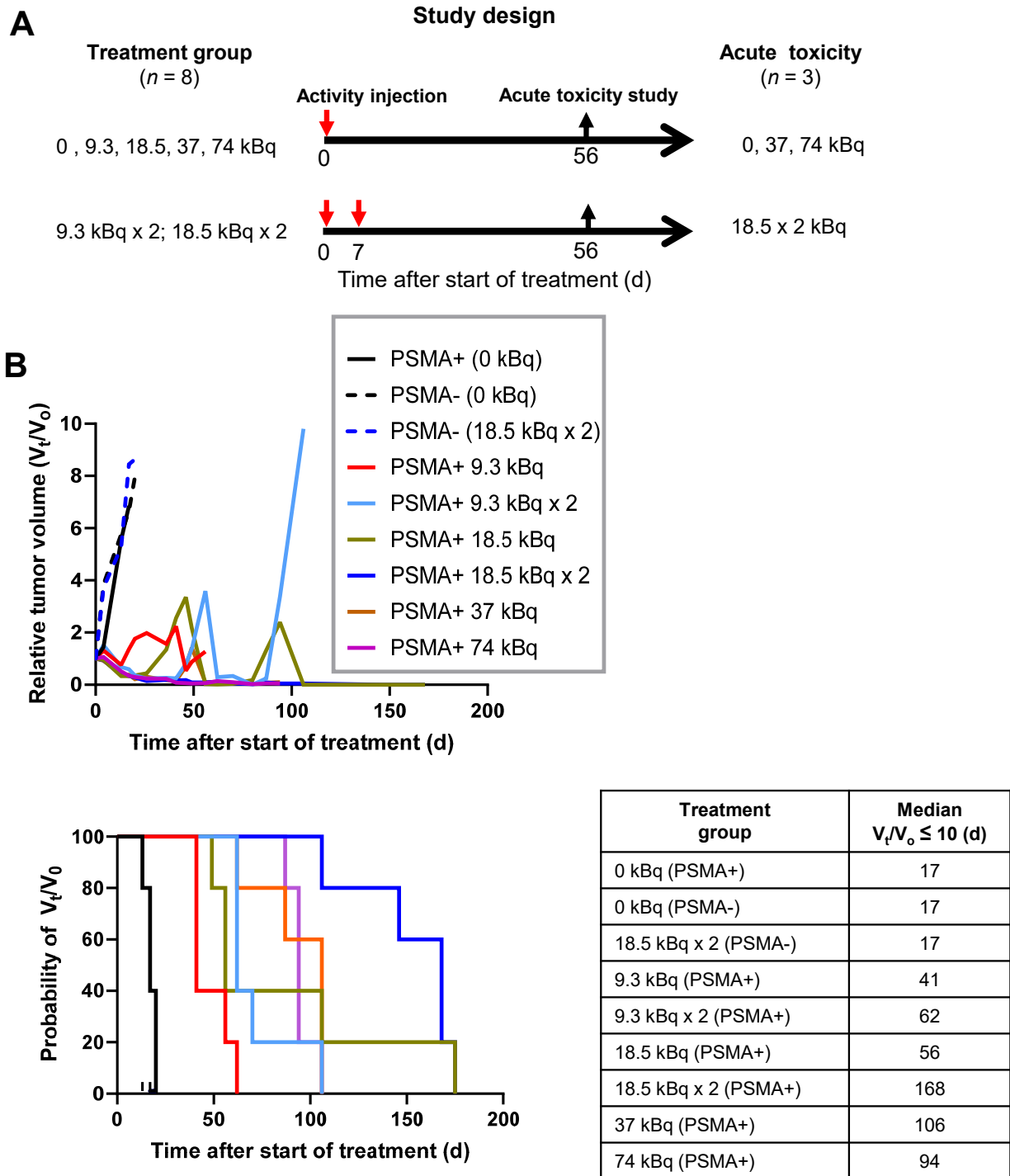
Figure 3. Activity-dependent radiopharmaceutical therapy of ^{225}Ac-L1 in mice bearing either PSMA+ or PSMA− PC3 flu flank tumors after administration via tail-vein injection (n=5). **A.** Study design; **B.** Relative tumor volume (V_t/V_o) (top); tumor growth curves relative to the tumor volume at Day 0 (set to 1); Kaplan–Meier curve illustrating time to grow $V_t/V_o \leq 10$ after treatment with ^{225}Ac-L1 or control (saline injection) (bottom).
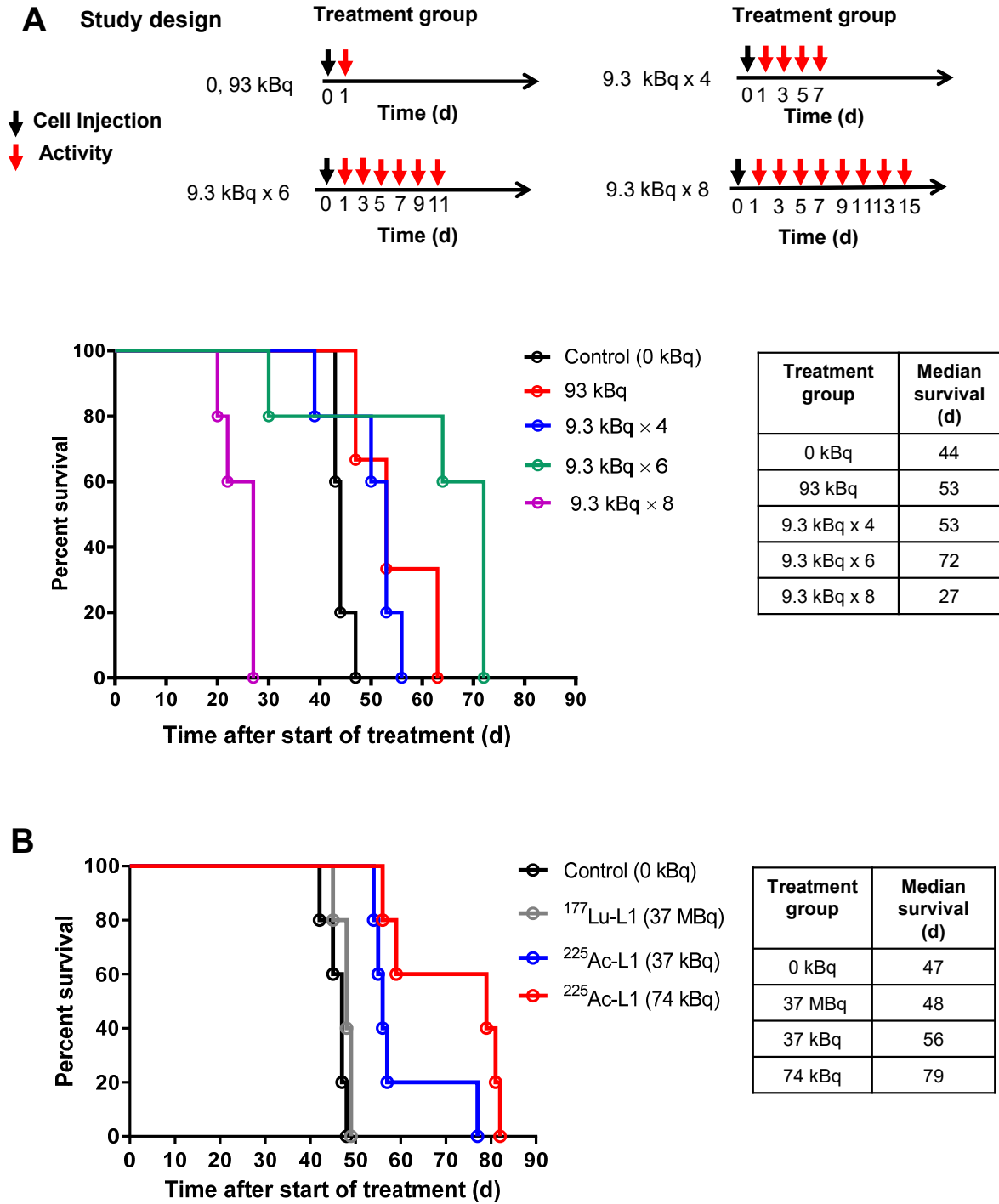
Figure 4. Treatment effect in PSMA+ micrometastatic model. **A.** Study design and Kaplan–Meier curve showing activity-dependent survival benefit after single and multiple administration. **B.** Kaplan–Meier curve showing improved survival after single administration of [225]Ac-L1 compared to [117]Lu-L1.
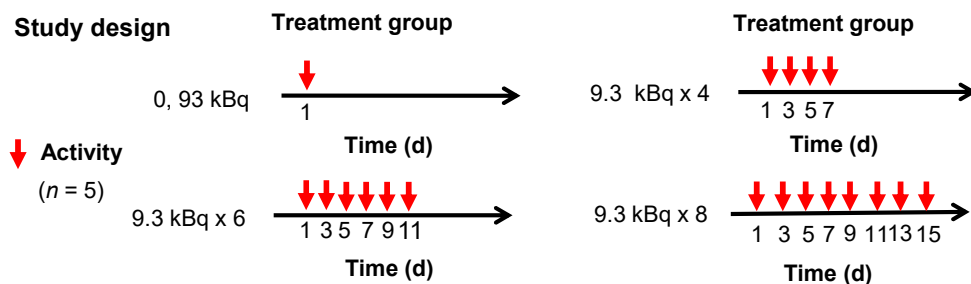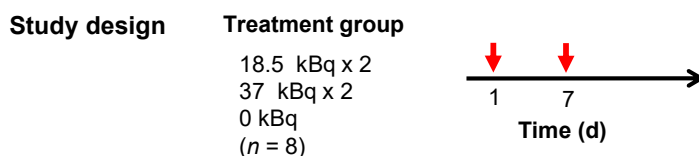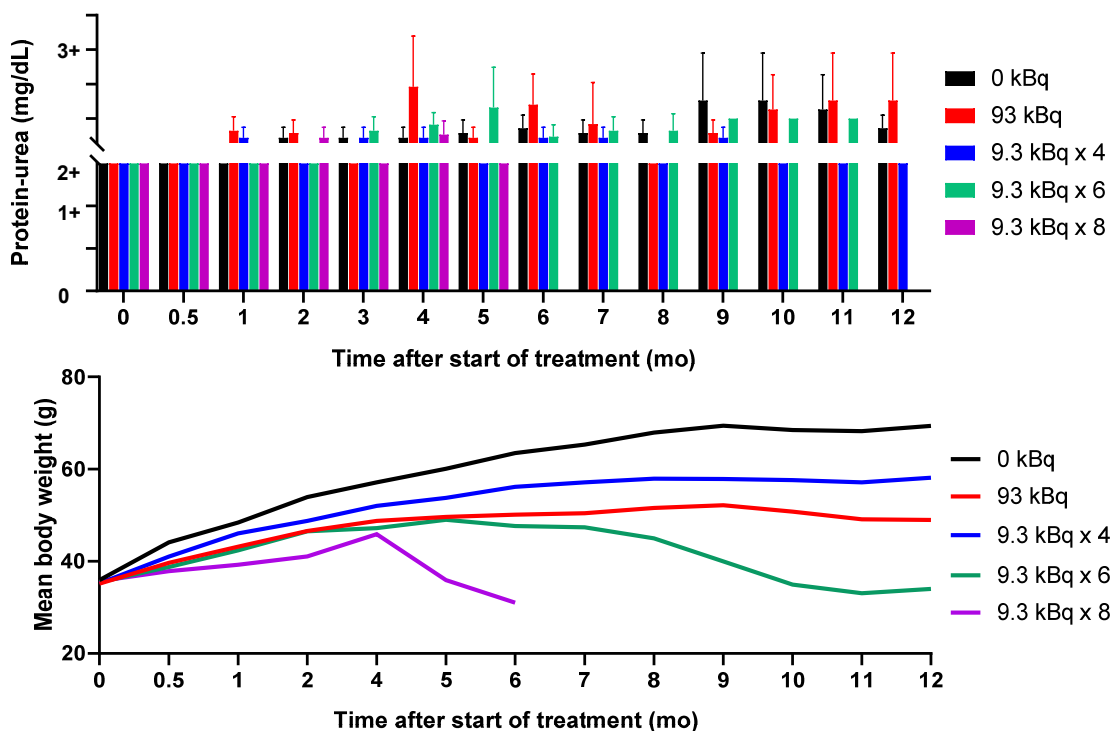
Figure 5. A. Study design (**1** and **2**) of the chronic and acute toxicity studies performed using immunocompetent CD-1 mice; **B.** Analysis of radiotoxicity parameters of ^{225}Ac-L1 in healthy CD-1 mice (n=5) for 1-12 months. Measured urine protein level by dipstick showed activity-dependent proteinuria occurring in the treatment groups (top) . Urine protein (trace, 0-10 mg/dL; 1+, 30 mg/dL; 2+, 100 mg/dL, 3+, 300 mg/dL) and Mean bodyweight (bottom).
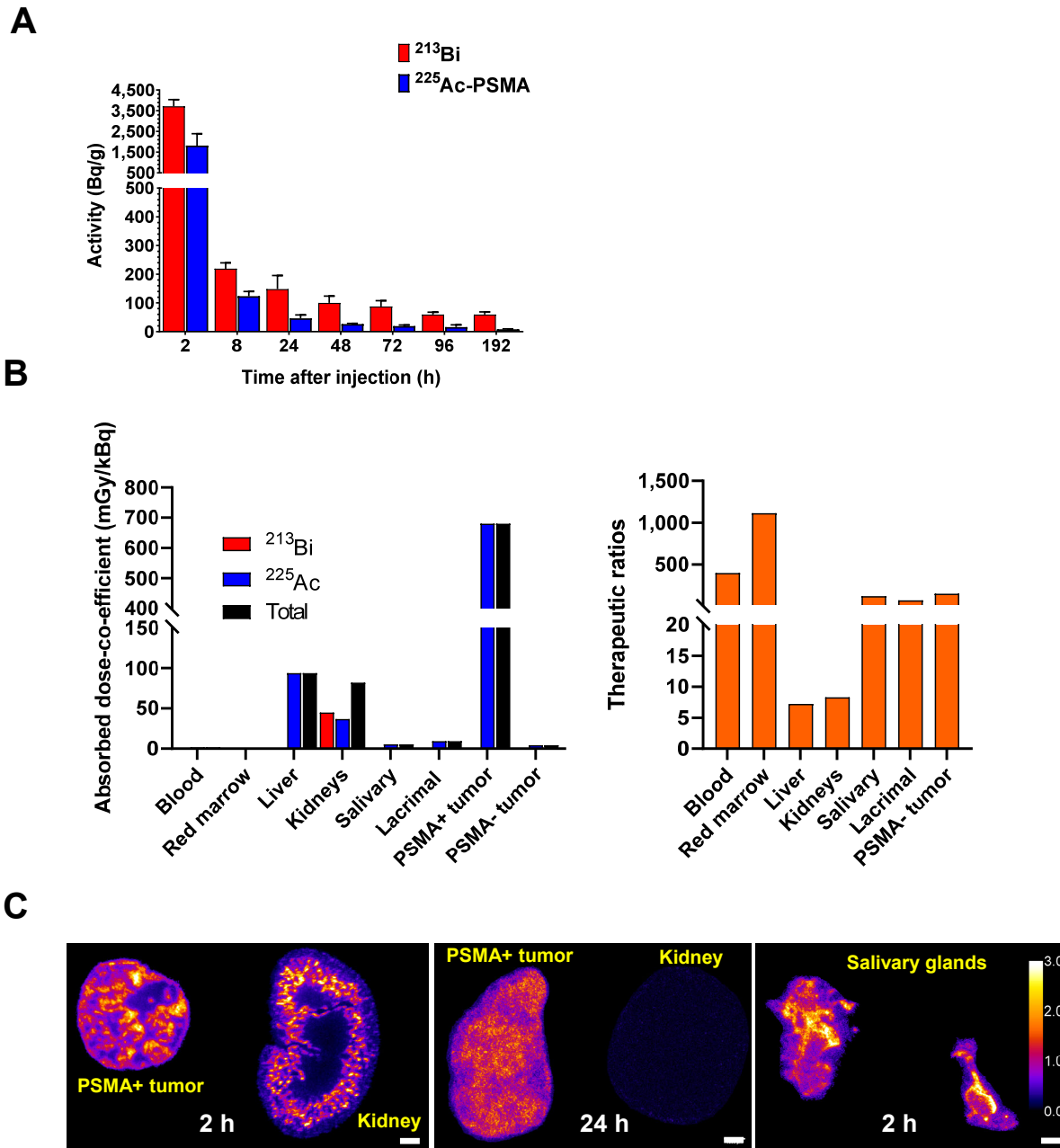
Figure 6. A. Activity per unit mass (Bq/g) within the kidneys of free in vivo generated ^{213}Bi and equilibrium ^{225}Ac-L1; **B.** Absorbed dose coefficient (ADC) of selected tissues and therapeutic ratio (ADC of PSMA+ tumor-to-normal organ); **C.** α-camera images (left and middle) showing sub-organ activity distribution within the kidney and in the tumor. Significant renal cortical clearance was observed after 24 h. (right) α-camera imaging of salivary glands (submandibular and parotid). The scale indicates the activity concentration normalized with the average activity in tumor 2h (left), tumor 24h (middle), and salivary glands 2 h (right). α-camera exposure:30 min (left and middle), 24 h (right).

GRAPHICAL ABSTRACT

$M = {}^{213}Bi/{}^{225}Ac$

PSMA+ PC3 PIP

Roadmap to translation

Cell uptake & Cell kill

Tissue biodistribution

Efficacy in flank tumor

Efficacy in micro-metastases

Long-term radiotoxicity

A. ^{225}Ac decay scheme

^{225}Ac

α   10.0 d

^{221}Fr

α   4.8 m

^{217}At

α   32.3 ms

^{213}Bi $\xrightarrow[\substack{97.84\% \\ 45.6 \text{ m}}]{\beta^-}$ ^{213}Po

α   2.16%
     45.6 m   α   4.2 μs

^{209}Tl $\xrightarrow[2.20 \text{ m}]{\beta^-}$ ^{209}Pb $\xrightarrow[3.253 \text{ h}]{\beta^-}$ ^{209}Bi
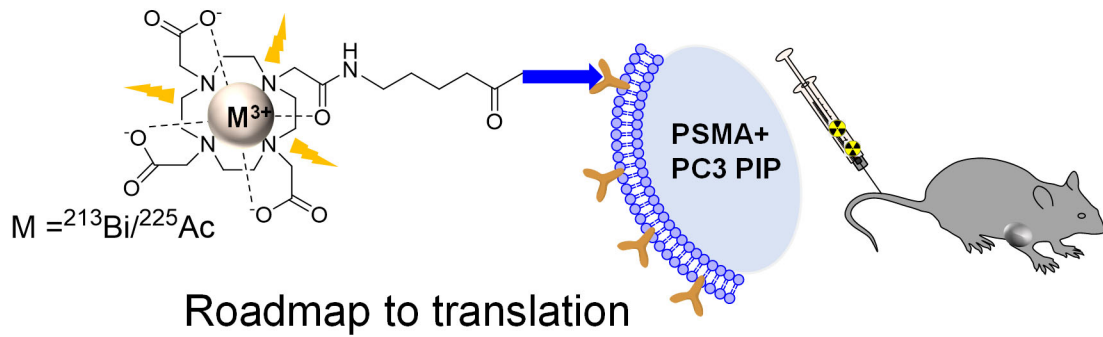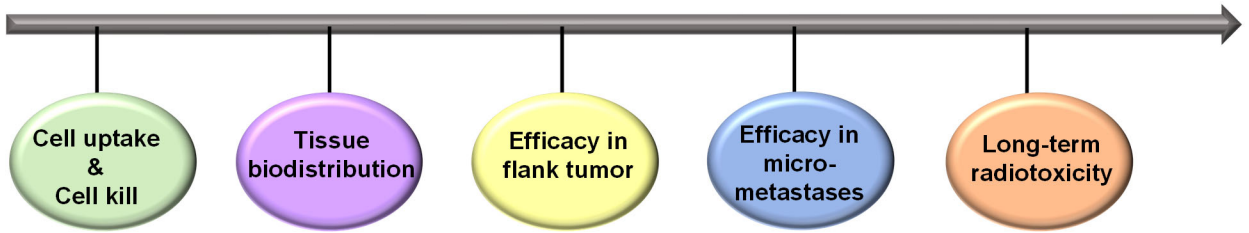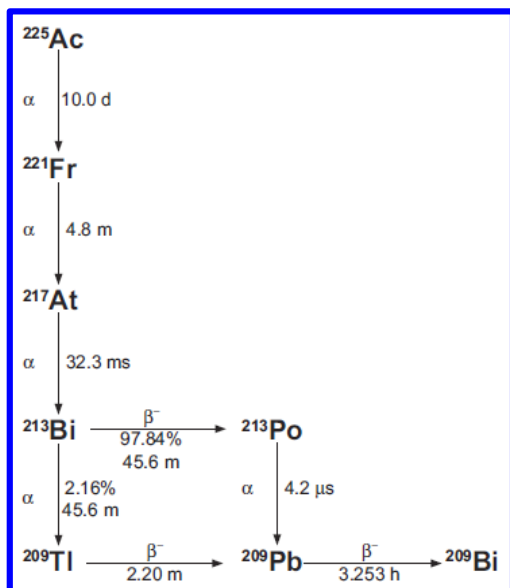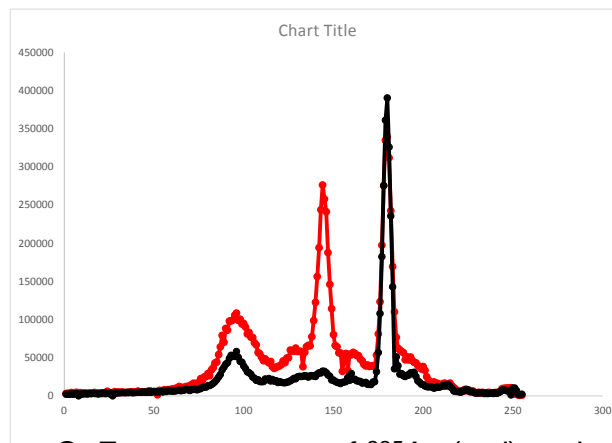
C. Energy spectra of ^{225}Ac (red) and ^{213}Bi (black) obtained after HPLC purification of ^{225}Ac-L1 from crude reaction.

^{213}Bi-L1

^{225}Ac-L1

^{213}Bi-L1

^{225}Ac-L1
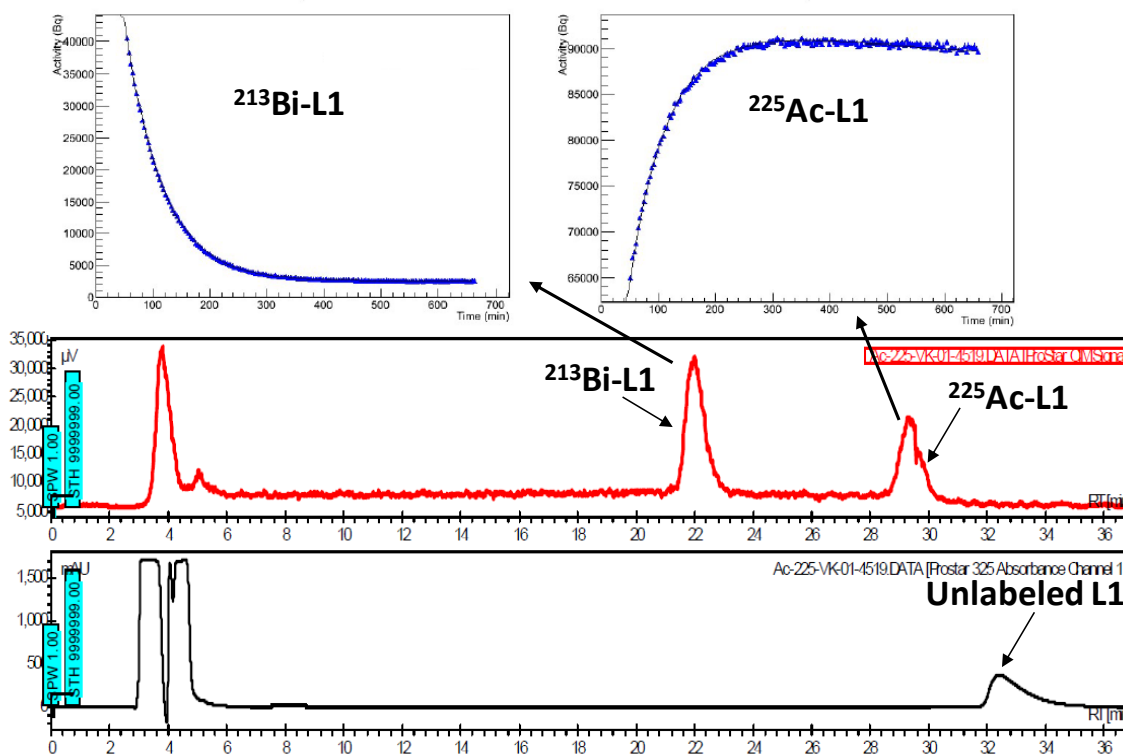
Unlabeled L1

B. HPLC chromatograms of ^{225}**Ac-L1** (red) and unlabeled ligand (black) from a crude reaction. HPLC peaks were further verified by gamma count fits (in blue, top) showing purity > 98% and gamma energy spectra shown in **C**.

A. HPLC chromatograms of ^{213}**Bi-L1** (red), unlabeled **L1** (black) from a crude reaction and ^{nat}**Bi-L1** (blue).
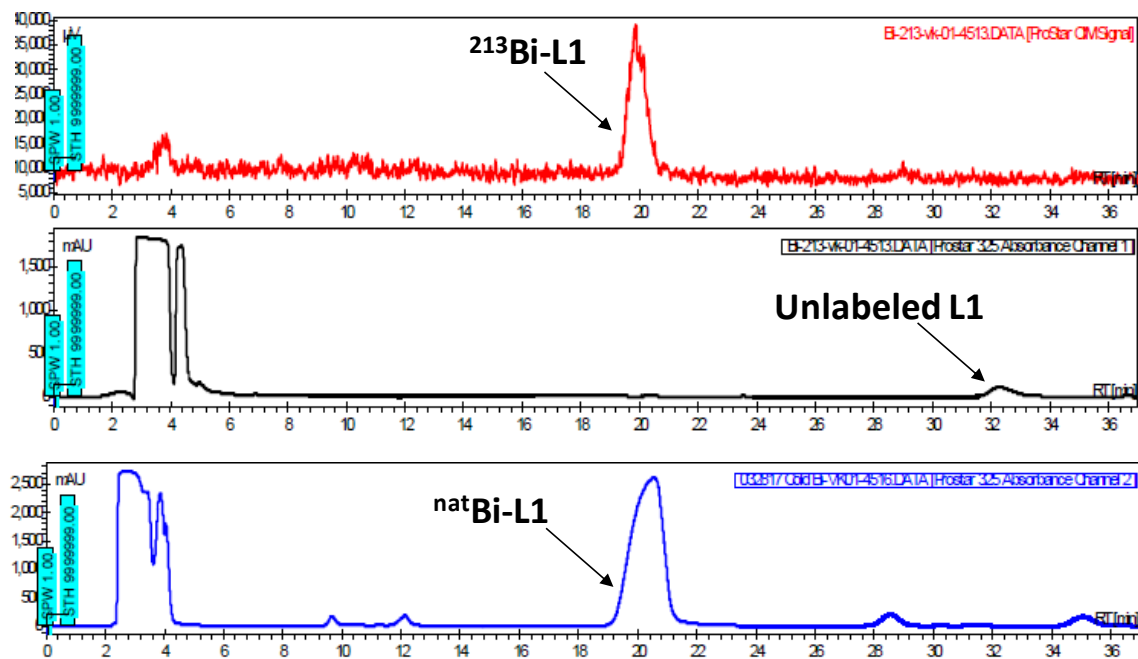
B. High-resolution electrospray ionization mass spectra of ^{nat}**Bi-L1**.
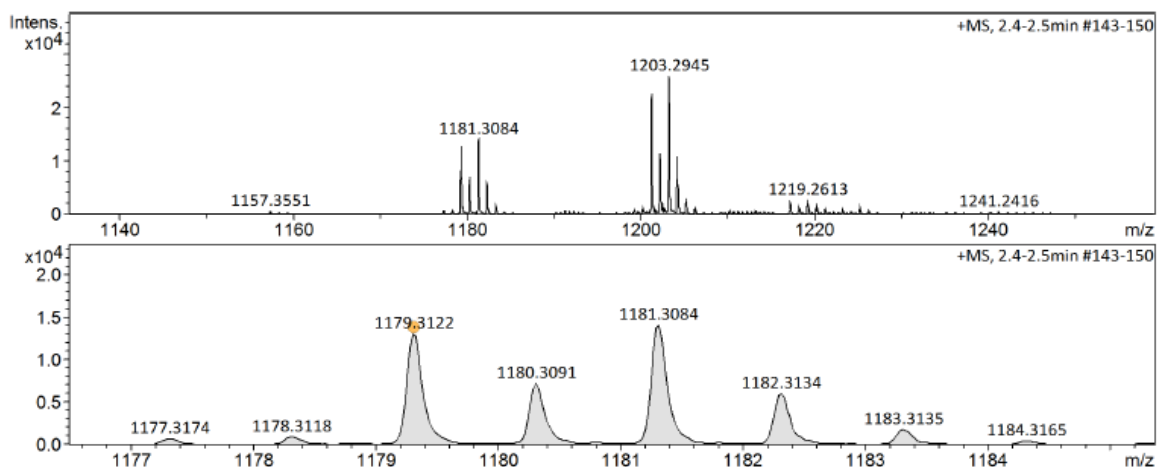
A. HPLC chromatogram of ^natLa-L1 (blue) and high-resolution electrospray ionization mass spectra of ^natLa-L1 (black).
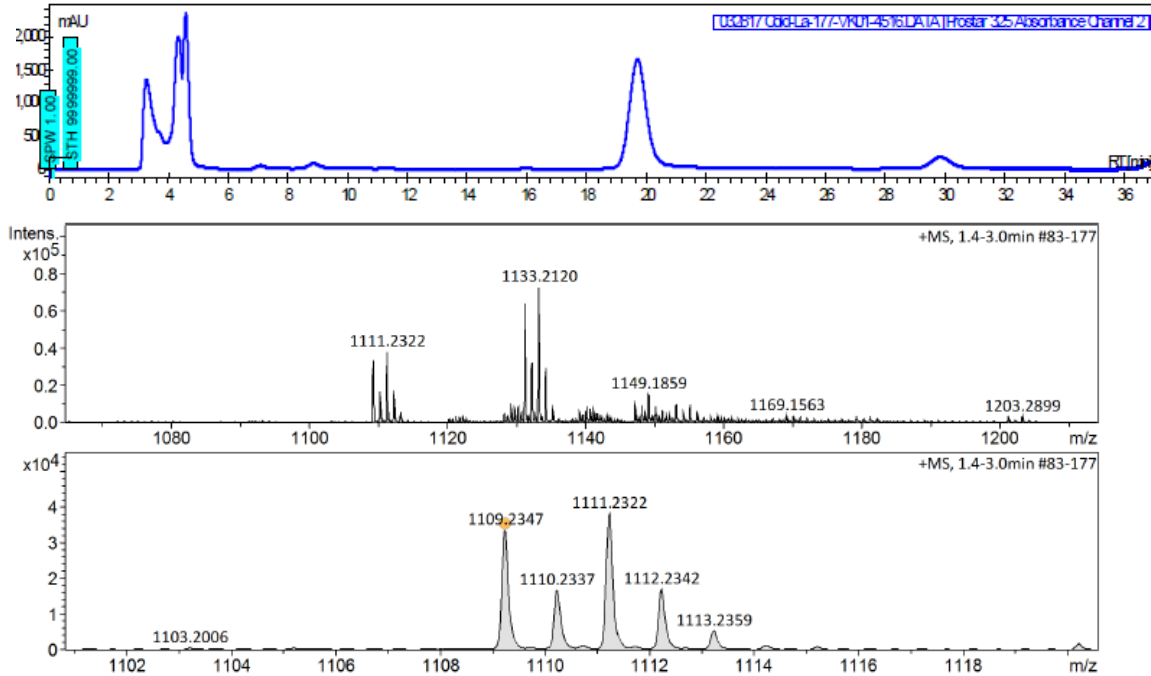
B. HPLC chromatogram of ^natLu-L1 (Top) and high-resolution electrospray ionization mass spectra of ^natLu-L1 (Bottom).
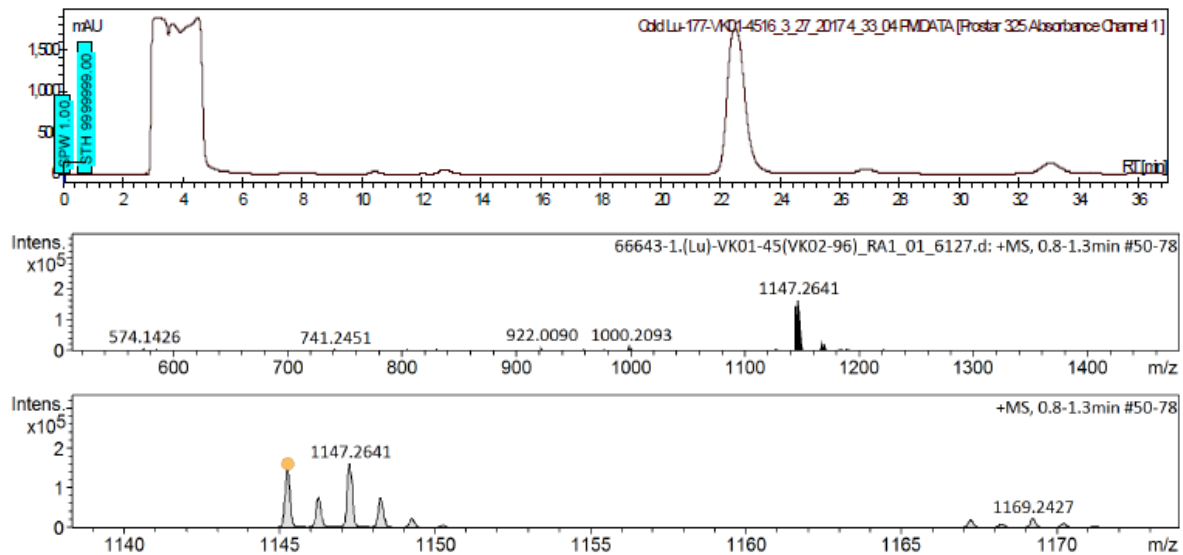
Supplemental Fig. 4. Treatment effect (V_t/V_0) of ^{213}**Bi-L1** in treated mice (3.7 MBq, single-administration) and the untreated mice with saline injection (PSMA+ PC3 PIP flank tumor model), experiment 6.
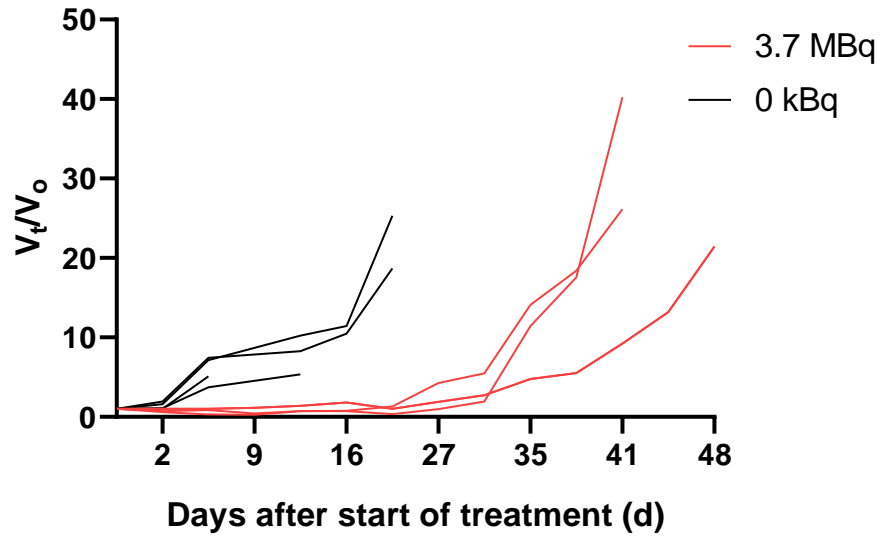
Supplemental Fig. 5. Treatment monitoring using in vivo bioluminescence
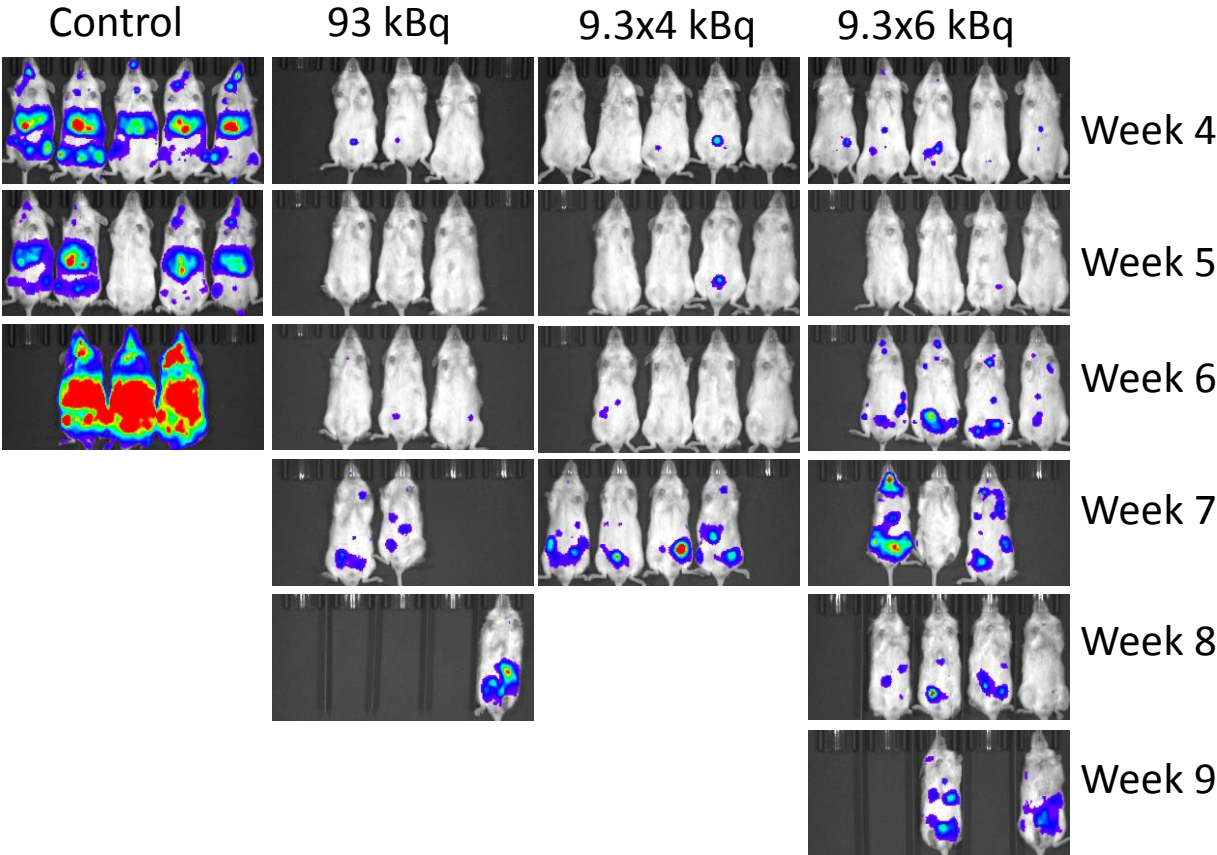
imaging in PSMA+ micrometastatic mode, after administration of ^{225}Ac-L1 (experiment 8).

Supplemental Figure 6A. H&E staining of kidneys of alive CD-1 mice after 12 months post-treatment (fractionated activity scheme, ^{225}Ac-L1, experiment 9).
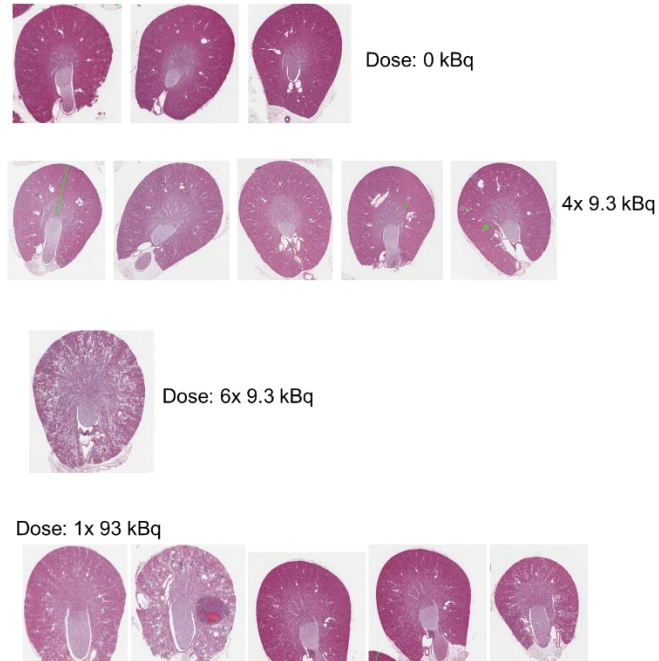
Supplemental Figure 6B. H&E staining of kidneys of alive CD-1 mice,12 months post-treatment (fractionated activity scheme, ^{225}Ac-L1, 93 kBq, experiment 9).
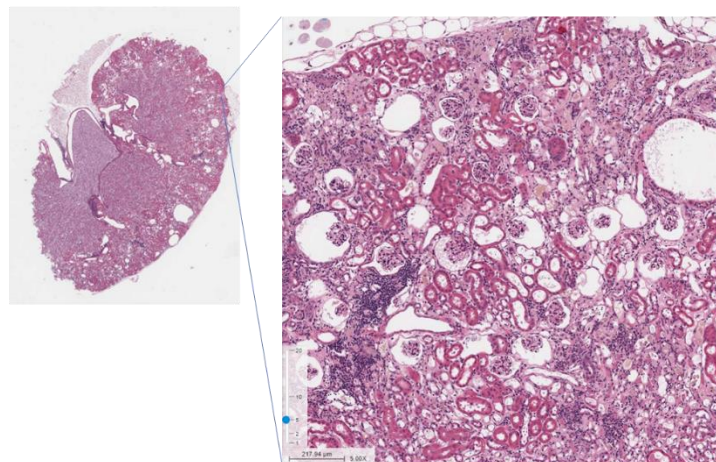
Supplemental Figure 7A-B. A. Selected blood counts and clinical chemistry data; B. Submandibular gland, H&E, (top) variations in cytoplasmic staining in both treated and control groups, with zymogen subjectively less prominent in treated group (n = 3). Parotid glands, H&E, (bottom left) mild variation in cytoplasmic staining.
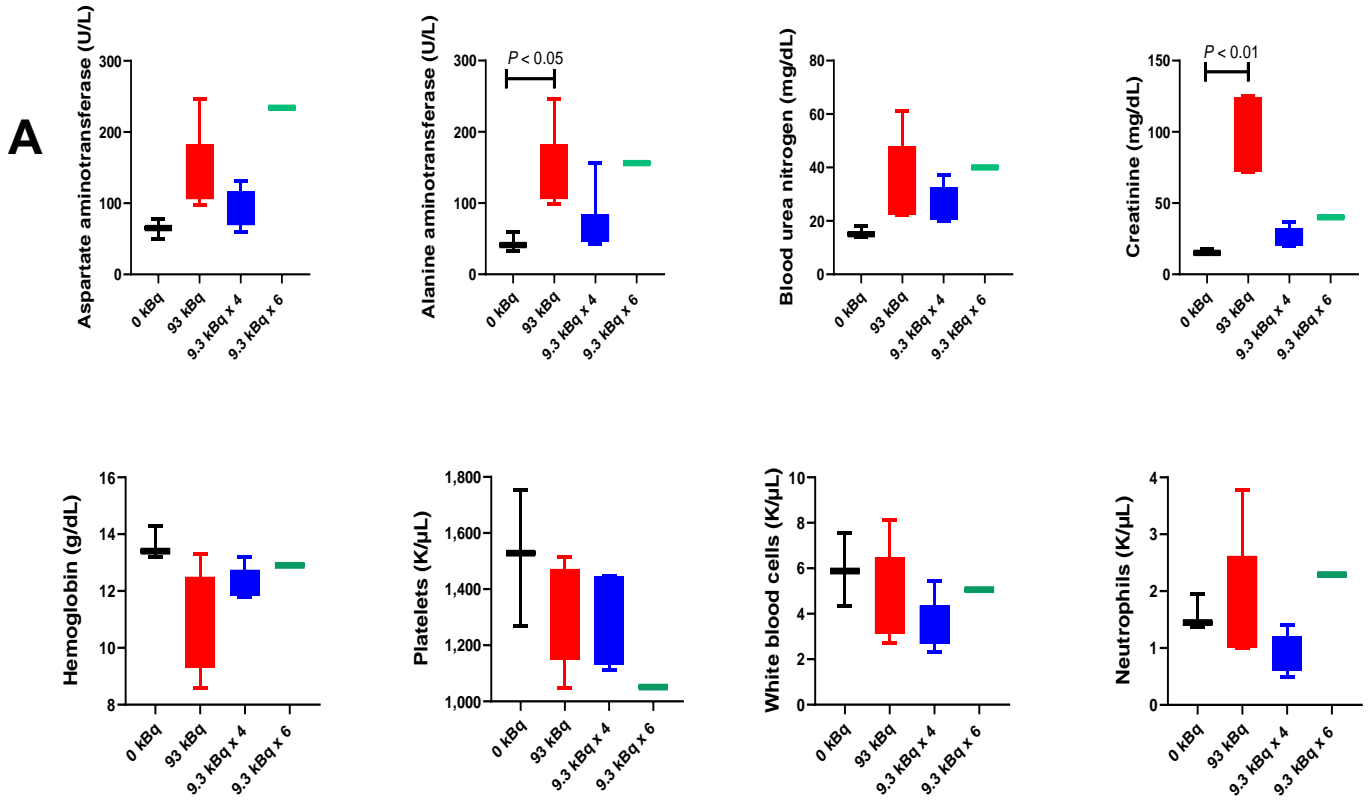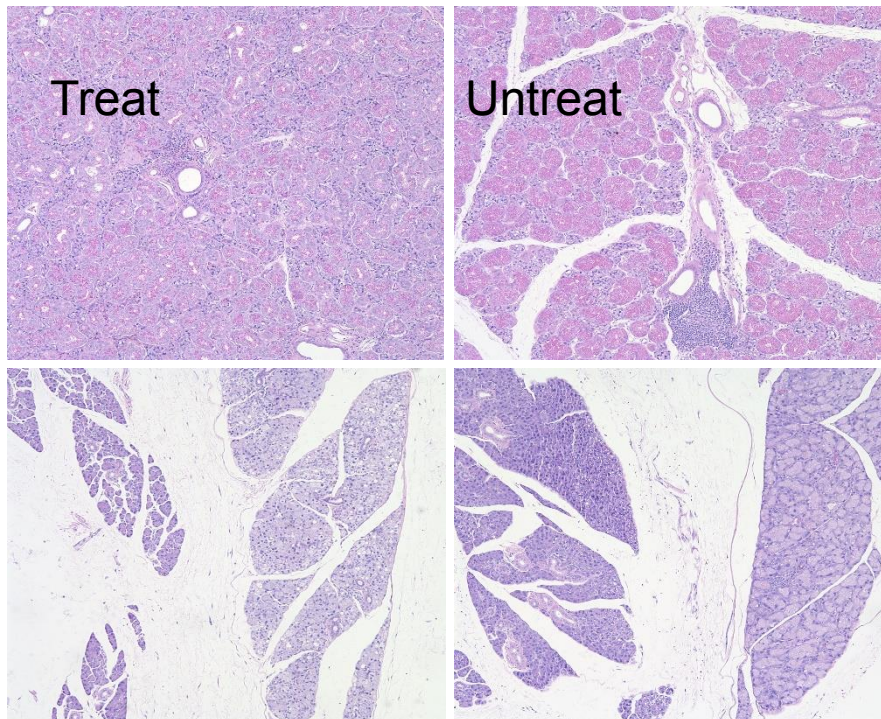
Supplemental Table 1. List of *in vivo* experiments performed in this report.

Experiment	Compound	Experiment name	Number of time-points	Number of mice/group	Total number of mice/study
1	^{213}Bi-L1	Tissue biodistribution study in tumor-bearing mice (male NSG mice)	(10, 30, 60, 120 min and, 60 min blocking)	4	16
2	^{225}Ac-L1	Tissue biodistribution study in tumor-bearing mice, counting done 24 h after sacrifice (male NSG mice)	2, 8, 24, 48, 72, 96, 120, 192 h	4	32
3	^{225}Ac-L1	Tissue biodistribution study in tumor-free mice (male CD-1 mice)	2, 24, 48, 72, 192 h	4	20
4	^{225}Ac-L1	Tissue biodistribution study in tumor-bearing mice, counting conducted immediately after sacrifice for determining kidney absorbed dose from free ^{213}Bi in the circulation (male NSG mice)	2, 8, 24, 48, 72, 96, 120, 192 h		
5	^{225}Ac-L1	Alpha-camera imaging using flank tumor model (male NSG mice)	2 and 24 h	2	4
6	^{213}Bi-L1	Efficacy studies in flank tumor model (male NSG mice)	PSMA+ tumor 3.7 MBq, 0 kBq	4	8
7A	^{225}Ac-L1	Activity-dependent efficacy studies in flank tumor model (male NSG mice)	Treatment group: PSMA+ tumor: 0 kBq 9.3 kBq 18.5 kBq 37 kBq 74 kBq 9.3 × 2 kBq 18.5 × 2 kBq (7 days apart). PSMA- tumor: 0 kBq 8.5 kBq × 2	8	72
7B	^{225}Ac-L1	Toxicity studies after 8 weeks PSMA+ flank tumor model (male NSG mice)	Used from the treatment groups from experiment 7A	3	NA
8	^{225}Ac-L1 vs. ^{177}Lu-L1	Activity-dependent treatment studies Micrometastatic model (male NSG mice)	Treatment group: **Study A** 0 kBq 92.5 kBq 9.3 × 4 kBq 9.3 × 6 kBq 9.3 × 8 kBq **Study B** 0 kBq 37 MBq (^{177}Lu-L1) 37 kBq 74 kBq	5	25 20
9	^{225}Ac-L1	Activity-dependent radiotoxicity studies used in micrometastatic model performed at 48 h interval (male CD-1 mice)	Treatment group: 0 kBq 92.5 kBq 9.3 × 4 kBq 9.3 × 6 kBq 9.3 × 8 kBq	5	25
10	^{225}Ac-L1	Activity-dependent radiotoxicity studies using fractionated activity scheme, administered 7 days apart (male CD-1 mice)	Treatment group: 0 kBq 18.5 × 2 kBq 37 × 2 kBq	5	15

Supplemental Table 2. Tissue biodistribution of ^{213}Bi-L1 using PSMA+ and PSMA-flank tumor-bearing male NSG mice. Data expressed in %ID/g (Mean ± SD), experiment number 1.

	10 min	30 min	1 h	2 h	1 h Blocking
Blood	5.13 ± 1.66	2.01 ± 1.29	1.06 ± 0.55	0.57 ± 0.00	2.24 ± 1.15
Heart	2.58 ± 0.66	0.60 ± 0.48	0.40 ± 0.04	0.43 ± 0.41	0.59 ± 0.15
Lung	4.73 ± 0.66	1.35 ± 1.21	1.00 ± 0.12	0.21 ± 0.08	1.51 ± 1.02
Liver	1.99 ± 0.21	0.57 ± 0.24	0.4 ± 90.10	0.29 ± 0.53	1.91 ± 0.09
Stomach	2.18 ± 0.63	0.77 ± 0.65	0.89 ± 0.74	0.04 ± 0.06	0.47 ± 0.15
Pancreas	1.48 ± 0.27	0.23 ± 0.65	0.78 ± 0.51	0.63 ± 1.37	0.45 ± 0.39
Spleen	2.80 ± 1.91	1.20 ± 1.77	1.34 ± 0.68	0.68 ± 1.27	0.82 ± 0.42
Fat	1.09 ± 1.06	0.08 ± 0.27	0.52 ± 0.33	0.33 ± 1.16	0.78 ± 1.24
Kidney	48.99 ± 21.18	23.07 ± 6.69	9.88 ± 1.83	8.60 ± 2.97	13.38 ± 2.43
Muscle	1.32 ± 0.22	0.53 ± 0.46	0.39 ± 0.16	0.11 ± 0.01	2.74 ± 5.15
Sm. Int.	2.29 ± 1.43	0.49 ± 0.71	0.74 ± 0.41	0.18 ± 0.25	0.71 ± 0.39
Sal. Glands	2.54 ± 0.77	0.14 ± 0.19	0.80 ± 0.42	0.93 ± 1.47	1.06 ± 1.03
Bladder	14.46 ± 14.14	1.63 ± 2.87	13.68 ± 11.65	1.45 ± 4.65	12.12 ± 5.59
Bone	2.38 ± 0.86	0.43 ± 0.84	2.70 ± 4.07	0.09 ± 0.71	1.96 ± 1.88
PSMA+ PIP	18.92 ± 3.14	19.34 ± 9.37	23.53 ± 4.15	29.36 ± 8.03	5.49 ± 0.64
PSMA- flu	±	±	ND	ND	ND
Tumor-to-blood	3.99±1.31	12.54±5.28	ND	ND	ND
Tumor-to-liver	9.57±3.13	50.82±47.12	ND	ND	ND
Tumor-to-salivary-gland	1.05±0.17	1.07±0.52	ND	1.7±0.48	ND
Tumor-to-kidney	0.43±0.14	0.78±0.40	ND	3.37±0.50	ND

Supplemental Table 3. Tissue biodistribution data of ^{225}Ac-L1 using male PSMA+ and PSMA- flank tumor-bearing NSG mice. Data expressed in %ID/g (Mean ± SD), experiment number 2.

	2 h	8 h	24 h	48 h	72 h	96 h	120 h	192 h
Blood	0.3 ± 0.3	0.1± 0.1	0.1 ± 0.0	0.1 ± 0.2	0.0 ± 0.1	0.1 ± 0.2	0.1 ± 0.1	0.0 ± 0.1
Heart	1.7 ± 2.3	0.4 ± 0.1	0.2 ± 0.1	0.1 ± 0.0	0.1 ± 0.1	0.1 ± 0.1	0.0 ± 0.0	0.0 ± 0.0
Lung	1.1 ± 0.6	0.4 ± 0.1	0.2 ± 0.0	0.1 ± 0.1	0.1 ± 0.0	0.1 ±0.0	0.0 ± 0.0	0.0 ± 0.0
Liver	2.7 ± 1.7	3.9 ± 1.1	3.1 ± 0.8	1.9 ± 0.9	1.6 ± 0.4	2.7 ±1.0	1.9 ± 0.5	2.1 ± 0.4
Stomach	0.9 ± 0.7	0.4 ± 0.2	0.4 ± 0.1	0.1 ± 0.1	0.1 ± 0.1	0.1 ± 0.1	0.1 ± 0.0	0.0 ± 0.1
Pancreas	0.6 ± 0.6	0.1 ± 0.0	0.0 ± 0.0	0.0 ± 0.0	0.0 ± 0.1	0.0 ± 0.0	0.1 ± 0.1	0.0 ± 0.0
Spleen	1.4 ± 1.2	0.6 ± 0.2	0.5 ± 0.5	0.4 ± 0.1	0.2 ± 0.3	0.5 ± 0.2	0.2 ± 0.1	0.3 ± 0.5
Fat	0.3 ± 0.3	0.2 ± 0.3	0.3 ± 0.1	0.2 ± 0.2	0.1 ± 0.1	0.1 ± 0.1	0.0 ± 0.0	0.0 ± 0.1
Kidney	27.5 ± 14.9	3.1 ± 0.9	1.5 ± 0.5	0.5 ± 0.4	0.5 ± 0.3	0.6 ± 0.4	0.3 ± 0.1	0.2 ± 0.2
Muscle	0.3 ± 0.2	0.1 ± 0.0	0.1 ± 0.1	0.1 ± 0.0	0.0 ± 0.1	0.0 ± 0.0	0.0 ± 0.0	0.0 ± 0.1
Sm. Int.	0.6 ± 0.4	0.3 ± 0.1	0.5 ± 0.5	0.1 ± 0.1	0.2 ± 0.2	0.0 ± 0.2	0.1 ± 0.1	0.3 ± 0.5
Sal. Glands	0.3 ± 0.1	0.1 ± 0.0	0.2 ± 0.1	0.1 ± 0.1	0.0 ± 0.1	0.1 ± 0.1	0.0 ± 0.0	0.0 ± 0.0
Laclm Gln	1.1± 1.1	0.5 ± 0.5	0.3 ± 0.2	0.2 ± 0.2	0.1 ± 0.2	0.1 ± 0.2	0.0 ± 0.1	0.1 ± 0.1
Bladder	2.4 ± 2.7	0.2 ± 0.1	0.5 ± 0.5	0.5 ± 0.4	0.0 ± 0.2	1.0 ± 1.3	0.0 ± 0.1	0.1 ± 0.2
Bone	0.8± 0.5	2.1 ± 10.0	0.5 ± 0.3	0.5 ± 0.4	0.2 ± 0.2	0.5 ± 0.4	0.5 ± 0.3	0.3 ± 0.3
PSMA+ PIP	45.8 ± 17.9	44.5 ± 12.9	49.0 ± 17.9	22.0 ± 7.5	18.3 ± 4.1	19.2 ± 6.4	12.6 ± 3.2	10.0 ± 2.2
PSMA- flu	0.6 ± 0.2	0.2 ± 0.1	0.3± 0.2	0.3 ± 0.2	0.1 ± 0.1	0.1 ± 0.1	0.1 ± 0.0	0.1 ± 0.1
Tumor-to-blood	222 ± 78	292 ± 96	592 ± 321	401 ± 122	N.D.	N.D.	N.D.	N.D.
Tumor-to-liver	12.8± 2.3	11.69 ± 1.9	15.3 ± 2.1	12.0 ± 2.8	11.2 ± 0.3	7.5 ± 2.10	6.5 ± 0.3	4.7 ± 0.4
Tumor-to-salivary-gland	164 ± 49.	347.7 ± 147.5	280.5 ± 89.5	235 ± 49	220.3 ± 62.3	110.8 ± 23.8	220 ± 112	420 ± 236
Tumor-to-kidney	1.9 ± 0.7	14.3 ± 1.1	33.9 ±8.6	48.0 ± 16.	39.5 ± 11.9	40.9 ± 15.0	41.7 ± 14.4	53.9 ± 18.2
Tumor-to-flu-tumor	79.3± 25.0	314.5 ± 185.8	203.8 ± 123	101.0 ± 64.3	242.5± 107.8	168.7± 33.5	147.9 ± 40.2	148 ± 75

Supplemental Table 4. Tissue biodistribution data of [225]Ac-L1 in male immunocompetent healthy CD-1 mice. Data expressed in %ID/g (Mean ± SD, n=4), experiment number 3.

	2 h	24 h	48 h	72 h	192 h
Blood	0.46 ± 0.11	0.05 ± 0.04	0.02 ± 0.02	0.00 ± 0.00	0.02 ± 0.03
Heart	0.20 ± 0.09	0.05 ± 0.03	0.03±0.05	0.05 ± 0.04	0.05 ± 0.04
Lung	0.59 ± 0.14	0.07 ± 0.02	0.04 ± 0.02	1.45 ± 0.63	0.14 ± 0.20
Liver	0.69 ± 0.25	0.40± 0.07	0.30 ± 0.02	0.02 ± 0.01	0.23 ± 0.07
Stomach	0.61 ± 0.52	0.06 ± 0.04	0.06 ± 0.02	0.01 ± 0.04	0.04 ± 0.08
Pancreas	0.89 ± 1.42	0.01 ± 0.02	0.05 ± 0.05	0.03 ± 0.04	0.02 ± 0.02
Spleen	0.53 ± 0.48	0.07 ± 0.06	0.11 ± 0.04	0.08 ± 0.06	0.17 ± 0.10
Fat	0.26 ± 0.24	0.04 ± 0.03	0.07 ± 0.05	0.28 ± 0.21	0.11 ±0.19
Kidney	39.10 ± 14.93	0.23 ± 0.09	0.15 ± 0.07	0.03 ± 0.04	0.05 ± 0.03
Muscle	0.32 ± 0.02	0.07 ± 0.03	0.03 ± 0.04	0.01 ± 0.04	0.12 ± 0.07
Sm. Int.	0.58 ± 0.19	0.15 ±0.05	0.11 ± 0.07	0.41 ± 0.31	0.23 ± 0.24
Saliv. Gland	0.31 ± 0.23	0.06 ± 0.00	0.03 ± 0.02	0.03 ± 0.06	0.13 ± 0.06
Bladder	10.05 ± 9.12	0.43 ± 0.27	0.27 ± 0.28	0.26 ± 0.09	0.39 ± 0.44
Bone	1.45 ± 1.31	0.16 ± 0.06	0.09 ± 0.03	0.11 ± 0.07	0.30 ± 0.24
Lacrimal gland	0.57 ± 0.41	0.43± 0.45	0.21 ± 0.12	0.27 ± 0.70	0.81 ± 0.98

Supplemental Table 5. A. Absorbed doses normalized to per injected activity (mGy/kBq) for the normal organs/tissues blood, red marrow, liver, kidneys, salivary glands, lacrimal glands, PSMA+ human PC3 PIP and PSMA- human PC3 flu- tumors. *Absorbed dose in mGy with contribution from unbound [213]Bi and [225]Ac-PSMA (n=4) (experiment number 4).

Organ/Tissue	[225]Ac-L1 (mGy/kBq)	[213]Bi (free) (mGy/kBq)	Total AD (mGy/kBq)
Blood	1.7	-	1.7
Red marrow	0.61	-	0.61
Liver	94	-	94
Kidney*	37	45	82
Salivary glands	5.5	-	5.5
Lacrimal glands	9.3	-	9.3
PC3 PSMA+ PIP tumor	680	-	680
PC3 PSMA- flu tumor	4.5	-	4.5

B. Selected Therapeutic ratios (PSMA+ tumor-to-normal organ ratio)

Blood	400
Red marrow	1115
Liver	7.2
Kidney*	8.3
Salivary glands	124
Lacrimal glands	73.1

C. Selected OLINDA/EXM data by conversion of mouse (35 g) to adult male phantom (73.7 kg)

Blood	510 MBq (limit 2 Gy)
Red marrow	1360 MBq (limit 2 Gy)
Liver	140 MBq (limit 32 Gy)
Kidney*	210 MBq (limit 40 Gy)
Total body	270 MBq (limit 2 Gy)
PC3 PSMA+ PIP tumor	31 MBq (tumor to reach 50 Gy)

Supplemental Table 6A. Complete blood count data after **8-weeks** from the treatment group administered with 18.5 kBq x 2, 37 kBq, 74 kBq and 0 kBq (n = 2) in PSMA+ **tumor-bearing NSG mice**, experiment number 7B.

	18.5 kBq x 2	18. 5 kBq x2	37 kBq	37 kBq	74 kBq	74 kBq	Control 0 kBq	Control 0 kBq
Red blood cells (M/µL)	8.38	9.21	8.61	7.89	8.36	8.58	10.03	9.56
Hemoglobin (g/dL)	13.00	14.40	13.40	12.30	12.80	13.50	15.30	14.40
Hematocrit %	45.50	49.20	46.60	42.40	43.60	46	53.20	49.60
Mean Corpuscular Value (MCV) fl	54.30	53.40	54.10	53.70	52.20	53.60	53	51.90
Mean Corpuscular Hemoglobin (MCH) pg	15.50	15.60	15.60	15.60	15.30	15.70	15.30	15.10
Reticulocytes (K/µL)	458.40	497.3	475.3	425.30	410.5	406.70	580.70	420.6
Reticulocytes %	5.47	5.4	5.52	5.39	4.91	4.74	5.79	4.40
Platelets (K/µL)	1220	1080	681	864	1221	1325	1533	1342
White blood cells (K/µL)	5.10	5.1	4.00	3.40	3.88	2.73	2.83	2.82
Neutrophils (K/µL)	3.26	2.88	1.49	1.72	1.76	1.34	1.37	1.17
Lymphocytes (K/µL)	1.46	1.52	1.13	1.16	1.09	1.04	1.17	1.09
Monocytes (K/µL)	0.27	0.50	1.2	0.31	0.88	0.17	0.13	0.39
Eosinophils (K/µL)	0.11	0.20	0.19	0.21	0.14	0.17	0.16	0.17
Basophil (K/ µL)	0	0.01	0.2	0	0.01	0.01	0	0

Supplementary Table S6B. Selected chemistry panel (metabolic profile) and lipid profile of the alive mice from the treatment group and organ perfused weight at 8 weeks post-treatment of the **tumor-bearing NSG mice**, experiment number 7B.

	18.5 kBq x 2	18. 5 kBq x2	37 kBq	37 kBq	74 kBq	74 kBq	Control	Control
Aspartate Aminotransferase (U/L)	56	110	91	110	84	148	85	321
Alanine Aminotransferase (U/DL)	23	30	44	39	31	25	27	88
Blood urea nitrogen (mg/dL)	25	24	25	31	24	23	29	30
Alkaline phosphatase U/L	46	59	52	60	51	43	58	45
Calcium (mg/dL)	10.8	10.2	10.7	10.6	10.4	10.4	11.3	10.5
Glucose (mg/dL)	260	231	255	301	253	257	246	248
Lactic Acid Dehydrogenase (U/L)	321	358	443	392	397	412	321	744
Gamma-Glutamyl transferase (U/L)	0	2	1	0	1	5	3	2
Total protein (g/dL)	5.2	5.7	5.5	5.4	5.4	5.3	5.6	5.3
Albumin (g/dL)	3	3.3	3.2	3.2	3.2	3.1	3.3	3.1
Total Bilirubin (mg/dL)	0.3	0.3	0.3	0.2	0.2	0.3	0.2	0.3
Creatinine (mg/dL)	0.5	0.5	0.4	0.5	0.3	0.3	0.3	0.4
Creatine Kinase (U/L)	123	349	246	403	208	618	289	1605
Phosphorous (mg/dL)	10.2	9.7	9.4	10.7	9.6	10.1	13.6	9.8
Magnesium (mg/dL)	2.9	3.2	3.2	2.6	2.4	2.5	3	2.3
Cholesterol (mg/dL)	105	92	97	81	85	95	145	117
Triglycerides (mg/dL)	137	130	78	76	92	118	91	104
Amylase (U/L))	1450	1201	1300	1343	1393	1364	1377	1319
Uric Acid (mg/dL)	3.5	2.9	3.3	2.6	3.6	2.8	3.8	3.4
High-density lipoprotein (mg/dL)	68	65	65	57	57	66	94	74
perfused								
Liver	2.06	1.72	1.88	1.68	1.84	1.64	1.75	1.73
LIVER: % of body weight	7.14	6.83	7.11	6.92	7.26	5.97	6.04	6.43
Spleen	0.04	0.05	0.05	0.05	0.05	0.04	0.03	0.05
SPLEEN: % of body weight	0.12	0.18	0.17	0.19	0.19	0.16	0.10	0.17
Heart	0.12	0.10	0.10	0.11	0.11	0.11	0.13	0.12
HEART: % of body weight	0.42	0.41	0.37	0.45	0.43	0.39	0.45	0.43
Right Kidney	0.26	0.25	0.25	0.23	0.22	0.30	0.26	0.27
Left Kidney	0.25	0.24	0.27	0.20	0.23	0.25	0.25	0.26
KIDNEYS: % of body weight	1.79	1.96	1.97	1.77	1.80	1.99	1.75	1.98

Supplementary Table S7A. Selected chemistry panel (metabolic profile) and lipid profile of the alive **tumor-free CD-1 mice** from the treatment group and organ perfused weight

at **8 weeks** post-treatment. (experiment number 10), Control * data were included form our previous report [Eur J Nucl Med Mol Imaging 2019;46:2545-57)].

	18.5 kBq x2	18.5 kBq x2	18.5 kBq x2	37 kBq x2	37 kBq x2	37 kBq x2	Control	Control	Control * (n=3)
Red blood cells (M/µL)	9.54	9.2	10.07	8.1	8.93	8.75	9.24	8.13	9.3 ± 0.0
Hemoglobin (g/dL)	14.4	15	15.6	12.9	14.1	13.8	13.4	12.9	14.0 ± 0.1
Hematocrit %	47.9	51	54.6	41.5	45.5	45.1	45	42.1	47.1 ± 1.1
Mean Corpuscular Value (MCV) fl	50.2	55.4	54.2	51.2	51	51.5	48.7	51.8	50.6 ± 1.0
Mean Corpuscular Hemoglobin (MCH) pg	15.1	16.3	15.5	15.9	15.8	15.8	14.5	15.9	15.0 ± 0.1
Reticulocytes (K/µL)	406.4	441.6	448.1	374.2	368.8	396.4	451.8	385.4	409.4 ± 107.1
Reticulocytes %	4.26	4.8	4.45	4.62	4.13	4.53	4.89	4.74	4.4 ± 1.1
Platelets (K/µL)	1200	1134	873	962	1207	1222	1368	1025	1503 ± 190.9
White blood cells (K/µL)	5.93	4.61	5.02	6.17	4.24	6.97	3.78	6.05	4.8 ± 0.8
Neutrophils (K/µL)	1.9	1.61	1.51	1.77	0.77	1.71	0.79	1.61	2.6 ± 0.1
Lymphocytes (K/µL)	3.74	2.81	3.3	4.11	3.31	4.32	2.73	4.07	1.7 ± 0.5
Monocytes (K/µL)	0.21	0.13	0.11	0.15	0.1	0.87	0.21	0.2	0.3 ± 0.2
Eosinophils (K/µL)	0.06	0.06	0.1	0.13	0.05	0.07	0.05	0.11	0.1 ± 0.0
Basophil (K/µL)	0.02	0	0	0.01	0.1	0	0	0.01	0.0 ± 0

Supplementary Table S7B. Selected chemistry panel (metabolic profile) and lipid profile of the alive mice from the treatment group administered and organ perfused weight at **8 weeks** post-treatment of the **tumor-free CD-1 mice** (experiment number 10). Control * data were included from our previous report [Eur J Nucl Med Mol Imaging 2019;46:2545-57)].

	18.5 kBq x2	18.5 kBq x2	18.5 kBq x2	37 kBq x2	37 kBq x2	37 kBq x2	Control	Control	Control*
Aspartate Aminotransferase (U/L)	83	106	58	132	127	156	54	105	123.5 ± 55.9
Alanine Aminotransferase (U/DL)	45	47	25	62	85	76	34	102	42.5 ± 20.5
Blood urea nitrogen (mg/dL)	17	20	21	23	16	16	21	25	25.5 ± 0.7
Alkaline phosphatase U/L	54	65	47	59	97	81	54	55	57.5 ± 0.7
Calcium (mg/dL)	9.7	9.6	10.8	10.2	10.1	10.8	10.5	10.4	11.6 ± 0.6
Glucose (mg/dL)	190	205	234	206	204	280	354	227	200.5 ± 3.5
Lactic Acid Dehydrogenase (U/L)	477	584	347	399	464	535	282	511	588.5 ± 89.8
Gamma-Glutamyl transferase (U/L)	2	3	2	3	4	4	4	5	3 ± 0
Total protein (g/dL)	5.8	6.1	5.5	5.1	5.5	5.9	6	5.7	5.7 ± 0.1
Albumin (g/dL)	3	3.2	2.9	2.8	2.9	3.2	3.2	3	3.1 ± 0.3
Total Bilirubin (mg/dL)	0.3	0.5	0.2	0.4	0.3	0.3	0.3	0.3	0.25 ± 0.1
Creatinine (mg/dL)	0.4	0.4	0.4	0.4	**0.5**	0.4	0.4	0.4	0.4 ± 0.1
Creatine Kinase (U/L)	234	331	142	209	231	404	70	169	274.5 ± 92.6
Phosphorous (mg/dL)	10.9	8.7	9.1	8.9	**10.2**	9.8	9.8	9.7	9.6 ± 0.2
Magnesium (mg/dL)	2.6	2.8	2.8	2.6	2.7	3.1	2.4	3.1	3.35 ± 0.2
Cholesterol (mg/dL)	182	133	202	122	156	177	199	180	121.5 ± 4.9
Triglycerides (mg/dL)	129	94	103	137	107	89	116	142	111.5 ± 21.9
Amylase (U/L))	1578	1484	1449	1276	1212	2938	1323	1565	1338 ± 107.5
Uric Acid (mg/dL)	2.3	3.2	3.2	2.5	2.5	3.3	3.6	2.4	3.1 ± 0.1
High-density lipoprotein (mg/dL)	118	91	111	69	92	98	98	114	78.5 ± 0.7

Supplementary Table S8A. Complete blood count data of the alive CD-1 mice from the treatment group administered with 9.3 kBq × 4 (48 h apart) (**M1-M5**) (n=5), 9.3 kBq x 6 (**M6**) (n=1) and control mice (saline treatment) (**MC1-MC3**) after **12** months, experiment number 9.

	M1	M2	M3	M4	M5	M6	MC1	MC2	MC3
Body Weight	48.626	50.759	58.765	60.166	60.009	30.334	71.763	58.058	50.865
Red blood cells (M/µL)	7.39	7.49	9.04	7.79	8.41	9.12	8.09	9.41	8.75
Hemoglobin (g/dL)	12	11.9	13.2	11.8	12.3	12.9	13.4	14.3	13.2
Hematocrit %	37.9	39.8	42.7	37.9	41.4	40.3	48.9	48.7	42.7
Mean Corpuscular Value (fl)	51.3	53.1	47.2	48.7	49.2	44.2	60.4	51.8	48.8
Mean Corpuscular Hemoglobin (pg)	16.2	15.9	14.6	15.1	14.6	14.1	16.6	15.2	15.1
Reticulocytes (K/µL)	315.6	362.5	514.4	323.3	344	457.8	2978.7	426.3	355.3
Reticulocytes %	4.27	4.84	5.69	4.15	4.09	5.02	36.82	4.53	4.06
Platelets (K/µL)	1110	1238	1445	1446	1152	1051	1267	1528	1754
White blood cells (K/µL)	2.33	3.11	5.45	3.27	3.03	5.06	7.55	5.88	4.34
Neutrophils (K/µL)	0.49	1.4	0.72	0.71	1.02	2.29	1.45	1.36	1.95
Lymphocytes (K/µL)	1.78	1.57	4.37	2.45	1.94	2.68	5.98	4.37	2.19
Monocytes (K/µL)	0.04	0.02	0.19	0.03	0.02	0.05	0.07	0.07	0.09
Eosinophils (K/µL)	0.02	0.12	0.17	0.08	0.04	0.02	0.04	0.08	0.11

Supplementary Table S8B. Selected chemistry panel (metabolic profile) and lipid profile of the alive mice from the treatment group administered with **9.3 kBq x 4** (48 h apart) (**M1-M5**), 9.3 kBq x 6 (**M6**) and control mice (**MC1-MC3**) (saline treatment) after 12 months and control untreated mice (saline treatment), experiment number 9.

	M1	M2	M3	M4	M5	M6	MC1	MC2	MC3
Aspartate Aminotransferase (U/L)	60	79	131	102	78	234	78	49	65
Alanine Aminotransferase (U/DL)	47	53	43	60	51	156	60	32	41
Blood urea nitrogen (mg/dL)	21	37	28	20	27	40	15	14	18
Creatinine (mg/dL)	33	77	66	65	43	250	87	41	35
Total protein (g/dL)	10.1	10.8	10.8	10.6	11	10.6	10.8	10.5	10.6
Albumin g/dL	211	188	252	218	226	162	150	196	241
Glucose (mg/dL)	458	486	699	598	473	271	471	259	330
Calcium (mg/dL)	5.0	3.0	3.0	3	2	6	3.0	3.0	2.0
Phosphorous (mg/dL)	5.4	6.1	5.9	6.1	6.2	6.7	6.7	5.8	6.2
Lactic Acid Dehydrogenase (U/L)	2.9	3.3	3.3	3.3	3.3	3.7	3.8	3.2	3.1
Creatine Kinase(U/L)	0.3	0.3	0.3	0.3	0.3	0.3	0.3	0.2	0.3
Alkaline phosphatase U/L	0.3	0.3	0.4	0.3	0.3	0.4	0.4	0.3	0.3
Total Bilirubin (mg/dL)	84	249	662	248	111	87	220	65	148
Gamma-Glutamyl transferase (U/L)	7.1	9.2	11	8.9	9.6	7.3	10.9	9.3	7.3
Magnesium (mg/dL)	157	158	158	156	158	156	164	155	153
Cholesterol (mg/dL)	8.1	10.2	9.7	7.8	8.3	8.1	7.5	8.5	9
Triglycerides (mg/dL)	118	120	117	116	119	120	117	114	115
Amylase (U/L)	2.7	3.2	3.7	3.1	3.2	3.7	3.8	2.8	3.5
Uric Acid (mg/dL)	141	204	222	180	263	199	193	117	192
High-density lipoprotein (mg/dL)	138	98	147	118	164	73	132	89	88
Direct Bilirubin (mg/dL)	1232	1181	1080	1183	1230	1162	1288	1383	1212
Aspartate Aminotransferase (U/L)	2.8	2.7	4.1	2.5	3	2.1	2.1	1.8	3.1
Alanine Aminotransferase (U/DL)	73	99	90	66	97	107	87	67	81

Supplementary Table S8C. Complete blood count data of the alive mice from the treatment group administered with 93 kBq (single administration) (M1-M5) and control mice (MC1, MC2, MC3) after 12 months, experiment number 9.

	M1	M2	M3	M4	M5	MC1	MC2	MC3
Body Weight	67.068	47.473	38.558	36.076	42.413	71.763	58.058	50.865
Red blood cells (M/µL)	9.02	7.15	8.1	7.48	5.86	8.09	9.41	8.75
Hemoglobin (g/dL)	13.3	10	11.7	11.4	8.6	13.4	14.3	13.2
Hematocrit %	43	32.8	36	35	25.4	48.9	48.7	42.7
Mean Corpuscular Value (MCV) fl	47.7	45.9	44.4	46.8	43.3	60.4	51.8	48.8
Mean Corpuscular Hemoglobin (MCH) pg	14.7	14	14.4	15.2	14.7	16.6	15.2	15.1
Reticulocytes (K/µL)	478.1	275.3	349.9	240.9	240.3	2978.7	426.3	355.3
Reticulocytes %	5.3	3.85	4.32	3.22	4.1	36.82	4.53	4.06
Platelets (K/µL)	1312	1432	1513	1046	1253	1267	1528	1754
White blood cells (K/µL)	3.91	3.5	4.83	2.73	8.1	7.55	5.88	4.34
Neutrophils (K/µL)	1	1.03	1.46	1.12	3.78	1.45	1.36	1.95
Lymphocytes (K/µL)	2.78	2.32	3.23	1.53	4.01	5.98	4.37	2.19
Monocytes (K/µL)	0.07	0.06	0.11	0.05	0.27	0.07	0.07	0.09
Eosinophils (K/µL)	0.06	0.08	0.02	0.02	0.04	0.04	0.08	0.11

Supplementary Table S8D. Selected chemistry panel (metabolic profile) and lipid profile of the alive mice from the treatment group administered with 93 kBq (single administration) (M1-M5) and control mice (MC1, MC2, MC3) after 12 months, experiment number 9.

	M1	M2	M3	M4	M5	MC1	MC2	MC3
Aspartate Aminotransferase (U/L)	**114**	**113**	**246**	**119**	**98**	78	49	65
Alanine Aminotransferase (U/DL)	**61**	**44**	**102**	**52**	**50**	60	32	41
Blood urea nitrogen (mg/dL)	**23**	**35**	**32**	**22**	**61**	15	14	18
Creatinine (mg/dL)	72	123	73	73	125	87	41	35
Total protein (g/dL)	10.9	11.4	9.9	10.1	11.3	10.8	10.5	10.6
Albumin g/dL	368	263	189	172	193	150	196	241
Glucose (mg/dL)	443	363	519	244	282	471	259	330
Calcium (mg/dL)	3	2	4	4	5	3.0	3.0	2.0
Phosphorous (mg/dL)	6.2	6.2	6.3	6	6	6.7	5.8	6.2
Lactic Acid Dehydrogenase (U/L)	3.3	3.4	3.2	3.3	3.1	3.8	3.2	3.1
Creatine Kinase(U/L)	0.2	0.2	0.3	0.2	0.2	0.3	0.2	0.3
Alkaline phosphatase U/L	**0.4**	**0.4**	**0.3**	**0.4**	**0.5**	0.4	0.3	0.3
Total Bilirubin (mg/dL)	564	333	201	62	384	220	65	148
Gamma-Glutamyl transferase (U/L)	11.6	8.3	7.6	9.5	8.5	10.9	9.3	7.3
Magnesium (mg/dL)	153	155	156	160	157	164	155	153
Cholesterol (mg/dL)	8.9	9.1	7.3	6.9	7.1	7.5	8.5	9
Triglycerides (mg/dL)	114	118	119	124	118	117	114	115
Amylase (U/L)	3.3	3.5	2.8	2.7	3.7	3.8	2.8	3.5
Uric Acid (mg/dL)	177	251	178	146	134	193	117	192
High-density lipoprotein (mg/dL)	108	112	159	143	96	132	89	88
Direct Bilirubin (mg/dL)	1506	1412	1374	1403	2182	1288	1383	1212
Aspartate Aminotransferase (U/L)	2.7	3.1	2.9	2.6	2.5	2.1	1.8	3.1
Alanine Aminotransferase (U/DL)	82	111	90	76	72	87	67	81

Supplementary Table S9A. Complete blood count data after 12 months for the alive mice (M1-M3) from the treatment group administered with 18.5 kBq x 2 (two administration, one week apart) (n = 3) and control mice (saline treatment) (n = 3), experiment number 10.

	M1	M2	M3	control	control	control
Red blood cells (10^6/uL)	8.44	6.37	2.26	9.31	10.63	9.99
Hemoglobin (g/dL)	12.4	9.7	4.2	13.7	16.4	15.1
Hematocrit %	38.8	29.5	14.1	43.6	55.1	49.7
Mean Corpuscular Value fl	46	46.3	62.4	46.8	51.8	49.7
Reticulocytes (K/µL)	402.6	402.6	635.7	437.6	547.4	477.5
Platelets (K/µL)	1598	721	436	1982	1454	1841
White blood cells (K/µL)	11.39	5.14	6.05	13.15	10.07	4.57
Neutrophils (K/µL)	3.08	2.6	0.45	3.22	3.18	1.18
Lymphocytes (K/µL)	6.5	2.33	4.79	3.62	6.17	2.79
Monocytes (K/µL)	1.54	0.11	0.78	0.71	0.46	0.46
Eosinophils (K/µL)	0.26	0.09	0.03	0.59	0.23	0.12

Supplementary Table S9B. Selected clinical chemistry data (metabolic profile and lipid profile) after 12 months of the alive mice (M1-M3) from the treatment group administered with 18.5 kBq x 2 (two administration, one week apart) and control mice (saline treatment) (n = 3), experiment number 10.

	M1	M2	M3	Control	Control	Control
Sodium (mmol/L)	161	N/A	150	161	158	163
potassium (mmol/L)	7.4	N/A	5.7	8.1	9.2	8.8
Chloride (mmol/L)	119	N/A	121	115	113	112
Aspartate Aminotransferase (U/L)	181	398	60	140	78	140
Alanine Aminotransferase (U/DL)	158	155	34	38	58	66
Blood urea nitrogen (mg/dL)	20	26	19	26	23	22
Creatinine (mg/dL)	0.3	0.3	0.3	0.6	0.5	0.5
Total protein (g/dL)	5.8	4.8	2.1	5.5	6.5	6.6
Albumin (g/dL)	2.8	2.9	1.3	2.7	3.5	3.3
Glucose (mg/dL)	140	102	171	161	203	232
Calcium (mg/dL)	10.1	10.1	8.5	10.3	11.8	11
Phosphorous (mg/dL)	6.8	6.1	5.3	14.7	13.3	10.6
Lactic Acid Dehydrogenase (U/L)	702	452	156	490	298	301
Creatine Kinase (U/L)	163	1097	178	845	187	419
Alkaline phosphatase U/L	260	86	34	21	70	46
Total Bilirubin (mg/dL)	0.3	0.6	0.6	0.3	0.3	0.3
Gamma-Glutamyl transferase (U/L)	3	3	2	0	0	0
Magnesium (mg/dL)	2.6	1.9	1.6	3.4	3.1	2.5
Cholesterol (mg/dL)	119	137	55	154	181	223
Triglycerides (mg/dL)	67	89	80	103	181	68
Amylase (U/L)	1150	5022	951	7343	1580	1026
Uric Acid (mg/dL)	3.1	3.1	1.7	3	2.6	3.2
High-density lipoprotein (mg/dL)	71	77	25	73	86	101
Organ Weights(g) perfused						
Liver	2.02	0.93	2.14	2.43	3.89	2.50
LIVER: % of body weight	5.30	3.82	3.76	5.33	6.41	5.22
Spleen	0.14	0.04	0.27	0.10	0.12	0.15
SPLEEN: % of body weight	0.36	0.15	0.47	0.22	0.20	0.31
Heart	0.19	0.16	0.22	0.23	0.26	0.24
HEART: % of body weight	0.49	0.64	0.38	0.50	0.43	0.50
Right Kidney	0.33	0.18	0.34	0.47	0.44	0.53
Left Kidney	0.27	0.22	0.34	0.44	0.46	0.46
KIDNEYS: % of body weight	1.55	1.63	1.19	2.00	1.48	2.06

Supplementary Table S9C. Complete blood count data for the alive mice from the treatment group administered with 37 kBq × 2 (one week apart of ^{212}**Ac-L1**) **at 195 days** after activity administration and control mouse (saline treatment), experiment number 10.

CBC	Control	M1	M2	M3	M4
Red blood cells (M/µL)	9.40	8.37	7.63	7.56	6.77
Hemoglobin (g/dL)	13.80	12.20	11.10	11.80	9.40
Hematocrit %	44.80	37.80	32.70	36.40	27.00
Mean Corpuscular Value (MCV) fl	47.70	45.20	42.90	48.10	39.90
Mean Corpuscular Hemoglobin (MCH) pg	14.70	14.60	14.50	15.60	13.90
Reticulocytes (K/µL)	414.50	384.20	491.40	384.80	213.90
Reticulocytes %	4.41	4.59	6.44	5.09	3.16
Platelets (K/µL)	1345.00	830.00	511.00	1063.00	780.00
White blood cells (K/µL)	6.11	10.35	5.44	9.53	5.73
Neutrophils (K/µL)	2.32	2.42	1.25	2.82	2.47
Lymphocytes (K/µL)	3.30	6.60	3.51	4.32	2.57
Monocytes (K/µL)	0.24	1.23	0.60	2.03	0.63
Eosinophils (K/µL)	0.24	0.09	0.08	0.35	0.04

Supplementary Table S9D. Selected chemistry panel (metabolic profile) and lipid profile of the alive CD-1 mice from the treatment group administered with 37 kBq × 2 (one week apart) **at 195 days** and control mice (saline treatment) (n = 3), experiment number 10.

	Control	M1	M2	M3	M4
Aspartate Aminotransferase (U/L)	86.00	218.00	530.00	427.00	157.00
Alanine Aminotransferase (U/DL)	59.00	135.00	347.00	443.00	87.00
Blood urea nitrogen (mg/dL)	22.00	22.00	22.00	25.00	51.00
Creatinine (mg/dL)	0.40	0.30	0.30	0.30	0.60
Total protein (g/dL)	6.00	5.90	5.40	5.90	5.50
Albumin g/dL	3.30	3.30	3.10	2.80	2.90
Glucose (mg/dL)	288.00	196.00	150.00	120.00	201.00
Calcium (mg/dL)	10.20	9.90	9.80	9.90	9.40
Phosphorous (mg/dL)	9.80	6.60	6.00	9.00	6.50
Lactic Acid Dehydrogenase (U/L)	350.00	475.00	852.00	1034.00	225.00
Creatine Kinase(U/L)	149.00	81.00	471.00	75.00	306.00
Alkaline phosphatase U/L	44.00	132.00	368.00	1773.00	184.00
Total Bilirubin (mg/dL)	0.30	0.30	0.50	1.10	0.20
Gamma-Glutamyl transferase (U/L)	2.00	4.00	4.00	5.00	3.00
Magnesium (mg/dL)	3.10	2.70	2.40	2.80	2.90
Cholesterol (mg/dL)	255.00	189.00	162.00	117.00	185.00
Triglycerides (mg/dL)	176.00	94.00	87.00	105.00	47.00
Amylase (U/L)	1256.00	1376.00	985.00	1110.00	1495.00
Uric Acid (mg/dL)	4.90	3.60	2.80	3.30	3.40
High-density lipoprotein (mg/dL)	117.00	123.00	99.00	58.00	146.00
Direct Bilirubin (mg/dL)	0.20	0.20	0.40	0.80	0.10